

1     **Chemical characterization of SOA formed from aqueous-phase reactions of phenols with**  
2                     **the triplet excited state of carbonyl and hydroxyl radical**

3  
4         Lu Yu<sup>1</sup>, Jeremy Smith<sup>2</sup>, Alexander Laskin<sup>3</sup>, Cort Anastasio<sup>2</sup>, Julia Laskin<sup>4</sup>, Qi Zhang<sup>1\*</sup>

5     <sup>1</sup>Department of Environmental Toxicology, University of California, 1 Shields Ave., Davis, CA  
6                                             95616, USA

7     <sup>2</sup>Department of Land, Air and Water Resources, University of California, 1 Shields Ave., Davis,  
8                                             CA 95616, USA

9     <sup>3</sup>Environmental Molecular Sciences Laboratory, Pacific Northwest National Laboratory,  
10                                             Richland, WA 99352, USA

11    <sup>4</sup>Physical Sciences Division, Pacific Northwest National Laboratory, Richland, WA 99352, USA

12  
13     \*Corresponding Author: Qi Zhang, Department of Environmental Toxicology, University of  
14     California, 1 Shields Ave., Davis, CA 95616, USA. Tel.: 530-752-5779; fax: 530-752-3394; e-  
15                                             mail: [dkwzhang@ucdavis.edu](mailto:dkwzhang@ucdavis.edu)

18 **Abstract**

19 Phenolic compounds, which are emitted in significant amounts from biomass burning,  
20 can undergo fast reactions in atmospheric aqueous phases to form secondary organic aerosol  
21 (aqSOA). In this study, we investigate the reactions of phenol and two methoxy-phenols  
22 (syringol and guaiacol) with two major aqueous phase oxidants – the triplet excited states of an  
23 aromatic carbonyl ( $^3C^*$ ) and hydroxyl radical ( $\bullet OH$ ). We thoroughly characterize the low-  
24 volatility species produced from these reactions and interpret their formation mechanisms using  
25 aerosol mass spectrometry (AMS), nanospray desorption electrospray ionization mass  
26 spectrometry (nano-DESI MS), and ion chromatography (IC). A large number of oxygenated  
27 molecules are identified, including oligomers containing up to six monomer units, functionalized  
28 monomer and oligomers with carbonyl, carboxyl, and hydroxyl groups, and small organic acid  
29 anions (e.g., formate, acetate, oxalate, and malate). The average atomic oxygen-to-carbon (O/C)  
30 ratios of phenolic aqSOA are in the range of 0.85-1.23, similar to those of low-volatility  
31 oxygenated organic aerosol (LV-OOA) observed in ambient air. The aqSOA compositions are  
32 overall similar for the same precursor, but the reactions mediated by  $^3C^*$  are faster than  $\bullet OH$ -  
33 mediated reactions and produce more oligomers and hydroxylated species at the point when 50%  
34 of the phenol had reacted. Profiles determined using a thermodenuder indicate that the volatility  
35 of phenolic aqSOA is influenced by both oligomer content and O/C ratio. In addition, the aqSOA  
36 shows enhanced light absorption in the UV-vis region, suggesting that aqueous-phase reactions  
37 of phenols may contribute to formation of secondary brown carbon in the atmosphere, especially  
38 in regions influenced by biomass burning.

39 Keywords: phenol, guaiacol, syringol, particulate matter, hydroxyl radical,  $^3C^*$ , SOA  
40 formation mechanisms, aqSOA

## 41 **1. Introduction**

42 Secondary organic aerosol (SOA) is ubiquitous in the atmosphere (Murphy et al., 2006;  
43 Zhang et al., 2007; Jimenez et al., 2009) and plays an important role in climate, human health,  
44 and air quality. Thus, understanding the impacts of SOA requires a thorough knowledge of the  
45 formation, evolution, and composition of SOA. This knowledge, however, is still limited because  
46 atmospheric organic chemistry is extremely complex. Numerous sources emit organic  
47 compounds and organic aerosol is formed and transformed via complicated chemical and  
48 physical processes in the atmosphere (Kanakidou et al., 2005).

49 SOA formation can take place in both gas and condensed phases. Much of the previous  
50 research on SOA has mainly focused on gas-phase reactions of volatile organic compounds  
51 (Hallquist et al., 2009). Recent work, however, has shown that SOA can also be produced  
52 efficiently in cloud and fog drops and water-containing aerosol (Blando and Turpin, 2000; Lim  
53 et al., 2005; Altieri et al., 2006; Ervens et al., 2011). Understanding the characteristics of SOA  
54 formed from aqueous-phase reactions (aqSOA) is important for properly representing its  
55 formation pathways in models and for elucidating its climatic and health effects.

56 Phenols are important precursors of aqSOA because 1) they are emitted in large  
57 quantities from biomass burning (Hawthorne et al., 1989; Schauer et al., 2001); 2) they have high  
58 Henry's Law constants and can partition significantly into atmospheric aqueous phases (Sagebiel  
59 and Seiber, 1993; Sander, 1999); and 3) they can undergo fast reactions with hydroxyl radical  
60 ( $\bullet\text{OH}$ ) and triplet excited states of organic compounds ( $^3\text{C}^*$ ) formed via light absorption by  
61 dissolved chromophores (Anastasio et al., 1997; Canonica et al., 2000; Smith et al., 2014). In the  
62 aqueous phase,  $\bullet\text{OH}$  is considered a dominant oxidant for organics. However, a recent study by  
63 Smith et al. (2014) showed that the destruction rates of phenols by  $^3\text{C}^*$  are comparable to or

64 faster than those by •OH under typical ambient conditions in areas influenced by biomass  
65 burning. An important source of  $^3\text{C}^*$  in the atmosphere is non-phenolic aromatic carbonyls – a  
66 group of compounds that are emitted from wood combustion in significant amounts (Hawthorne  
67 et al., 1992; Simoneit et al., 1999) and have been detected in fog and cloud droplets  
68 (Leuenberger et al., 1985; Sagebiel and Seiber, 1993). These compounds, once dissolved in  
69 water, can absorb light to form  $^3\text{C}^*$  and catalyze the oxidation of phenols with little or no loss of  
70 the aromatic carbonyl (Anastasio et al., 1997; Smith et al., 2014). This is an indication that non-  
71 phenolic aromatic carbonyls, along with a number of other organic compounds recently reported  
72 (Monge et al., 2012; Aregahegn et al., 2013; Rossignol et al., 2014), can act as photosensitizer to  
73 promote SOA formation in atmospheric condensed phases.

74 According to recent studies, phenols react with •OH and  $^3\text{C}^*$  to form aqSOA with mass  
75 yields close to 100% (Smith et al., 2014), making reaction products that include small organic  
76 acids, hydroxylated phenols, and oligomers (Sun et al., 2010). However, since Sun et al. (2010)  
77 mainly used an Aerodyne high-resolution time-of-flight aerosol mass spectrometer with an  
78 electron impact (EI) ionization source, in which analyte molecules are generally extensively  
79 fragmented (Canagaratna et al., 2007), the molecular composition of the phenolic aqSOA was  
80 not sufficiently characterized. In addition, since Sun et al. (2010) examined phenol reactions only  
81 with •OH, almost nothing is known about the chemistry of aqSOA formed from  $^3\text{C}^*$  reactions.

82 In this study, we thoroughly characterize the aqueous reaction products of phenols with  
83  $^3\text{C}^*$  produced from a non-phenolic aromatic carbonyl and •OH from hydrogen peroxide (HOOH)  
84 under simulated sunlight illumination. We studied three basic structures of biomass-burning  
85 phenols – phenol ( $\text{C}_6\text{H}_6\text{O}$ ), guaiacol ( $\text{C}_7\text{H}_8\text{O}_2$ ; 2-methoxyphenol), and syringol ( $\text{C}_8\text{H}_{10}\text{O}_3$ ; 2,6-  
86 dimethoxyphenol). We examine the molecular and bulk compositions of low-volatility species

87 produced from these reactions and use this information to interpret the formation pathways of  
88 phenolic aqSOA.

## 89 **2. Experimental Methods**

### 90 *2.1 Phenolic aqSOA samples*

91 The aqSOA samples of phenol, guaiacol, and syringol were prepared during simulated  
92 sunlight illumination under two oxidant conditions: (1) via reaction with  $^3\text{C}^*$  formed from 5  
93  $\mu\text{mol L}^{-1}$  3,4-dimethoxybenzaldehyde (3,4-DMB) and (2) via reaction with  $\bullet\text{OH}$  generated from  
94  $100 \mu\text{mol L}^{-1}$  hydrogen peroxide (HOOH; Table 1). 3,4-DMB was chosen as the photosensitizer  
95 in this study to represent non-phenolic aromatic carbonyls, which are emitted in large quantities  
96 from wood burning (Schauer et al., 2001), exist nearly exclusively in condensed phases in the  
97 atmosphere, and rapidly form  $^3\text{C}^*$  that efficiently oxidizes phenols (Anastasio et al., 1997).  
98 Details of the experiments are reported in Smith et al. (2014) and a brief summary is given here.  
99 Initial solutions were composed of air-saturated Milli-Q water (resistance  $> 18 \text{ M}\Omega\text{-cm}$ ;  
100 Millipore) containing  $100 \mu\text{mol L}^{-1}$  of a single phenol and adjusted to  $\text{pH} = 5$  using sulfuric acid.  
101 Each solution was illuminated in an RPR-200 Photoreactor System (George et al., 2014) until  
102 approximately half of the initial phenol was degraded (as monitored by a high performance  
103 liquid chromatograph (HPLC) with a UV-vis detector). At that point, 12.0 mL of the illuminated  
104 solution was placed in an aluminum cup and blown gently to dryness with pure  $\text{N}_2$  at room  
105 temperature. Another aliquot of the illuminated solution was flash frozen with liquid nitrogen  
106 and stored at  $-20 \text{ }^\circ\text{C}$  in the dark until analysis. Note that the flash-frozen samples contain  
107 dissolved volatile species, low-volatility species and unreacted precursors, while the blown-down  
108 samples are composed of only low-volatility species. Indeed, HPLC analysis of the blown-down  
109 samples detected negligible amounts of the initial phenols, indicating that they were completely

110 removed. In addition, all phenolic precursors show first-order decay during photoreactions to a  
111 time of one half-life (Smith et al., 2014), indicating that the reaction intermediates or products  
112 are not acting as significant photosensitizers. The phenol precursors themselves are not effective  
113 photosensitizers since they have little or no light absorption in the solar range (Smith et al., 2014).  
114 Dark control experiments, carried out under the same condition except in the dark, showed  
115 negligible loss of phenol and no formation of aqSOA. In addition, no formation of aqSOA was  
116 observed in control experiments in which 3,4-DMB was illuminated alone under the same  
117 condition and the resulting solution evaporated in the same way.

## 118 ***2.2 Analytical methods***

### 119 *2.2.1 Aerosol Mass Spectrometry (AMS) measurement and data analysis*

120 In this study, a High Resolution Time-of-Flight Aerosol Mass Spectrometer (Aerodyne  
121 Res. Inc., Billerica, MA; thereafter referred to as AMS) was used to characterize the bulk  
122 chemical composition and elemental ratios of the low-volatility substances in both blown-down  
123 and flash-frozen samples. The working principles of the AMS have been discussed previously  
124 (DeCarlo et al., 2006; Canagaratna et al., 2007). Briefly, the AMS analyzes nonrefractory  
125 aerosols that evaporate at  $\sim 600$  °C under high vacuum via 70 eV EI mass spectrometry. In this  
126 study, the AMS was operated alternatively between “V” and “W” ion optical modes (mass  
127 resolutions of  $\sim 3000$  and  $\sim 5000$ , respectively) to acquire mass spectra up to  $m/z$  500 and  $m/z$   
128 300, respectively. Prior to AMS analysis, each blown-down sample was dissolved in 6.0 mL  
129 Milli-Q water and the flash-frozen samples were thawed overnight inside a refrigerator ( $\sim 4$  °C).  
130 The liquid samples were atomized in argon (Industrial Grade, 99.997%) using a constant output  
131 atomizer coupled with a diffusion dryer and the resulting particles were analyzed by the AMS  
132 downstream of a digitally controlled thermodenuder (TD) (Fierz et al., 2007). The TD consists of

133 a bypass line and a heated line terminating in a section with activated carbon cloth. The  
134 temperature inside the heated line was programmed to cycle through 7 different temperatures (25,  
135 40, 65, 85, 100, 150, and 200 °C) every hour. An automated 3-way valve switched the sample  
136 flow between bypass and TD modes every 5 min. By comparing the measurements between  
137 these two modes, we can determine the volatility profiles of the aqSOA. Between every two  
138 sample runs, Milli-Q water was atomized and analyzed as an analytical blank.

139 The AMS data were analyzed using the AMS data analysis software (SQUIRREL v1.12  
140 and PIKA v1.53 downloaded from [http://cires.colorado.edu/jimenez-](http://cires.colorado.edu/jimenez-group/ToFAMSResources/ToFSoftware/)  
141 [group/ToFAMSResources/ToFSoftware/](http://cires.colorado.edu/jimenez-group/ToFAMSResources/ToFSoftware/)). The W-mode data was analyzed to determine the  
142 atomic ratios of oxygen-to-carbon (O/C) and hydrogen-to-carbon (H/C) and the organic mass-to-  
143 carbon ratio (OM/OC) of phenolic aqSOA (Aiken et al., 2008). V-mode data were analyzed for  
144 information of higher molecular weight ions with  $m/z > 300$ , such as syringol dimer  $C_{16}H_{18}O_6^+$   
145 ( $m/z$  306) and guaiacol trimer  $C_{21}H_{20}O_6^+$  ( $m/z$  368). Note that accurately quantifying the organic  
146 contributions to the  $H_2O^+$ ,  $CO^+$ , and  $CO_2^+$  signals in an ensemble mass spectrum is critical to the  
147 determination of the O/C and H/C ratios of an organic aerosol (Aiken et al., 2008; Sun et al.,  
148 2009; Collier and Zhang, 2013). Since Ar was used as the carrier gas for atomization,  $N_2$  and  
149  $CO_2$  did not interfere with the quantification of the organic  $CO^+$  and  $CO_2^+$  signals. In terms of the  
150  $H_2O^+$  signal, contribution from gaseous water molecules was negligible because the relative  
151 humidity measured at the AMS inlet was very low (< 2%). In addition, since heating the aerosol  
152 to 40 °C prior to AMS sampling led to almost no change in the relative intensities of the  $H_2O^+$   
153 signal in the mass spectra of aqSOA (Fig. S1 in the supplementary information), particles  
154 appeared to be completely dry. The organic portion of the  $H_2O^+$  signal was thus determined as

155 the difference between the measured  $\text{H}_2\text{O}^+$  signal and the sulfate-associated  $\text{H}_2\text{O}^+$  signal  
156 estimated according to the known fragmentation pattern of sulfates (Allan et al., 2004).

157 *2.2.2 Nanospray Desorption Electrospray Ionization Mass Spectrometry (nano-DESI MS)*  
158 *measurement and data analysis*

159 Prior to nano-DESI MS analysis, the blown-down samples of phenolic aqSOA were  
160 dissolved in Milli-Q water, atomized, and collected on Teflon membrane filters. The analyses  
161 were performed using a high-resolution LTQ-Orbitrap mass spectrometer (Thermo Electron,  
162 Bremen, Germany) with a resolving power ( $m/\Delta m$ ) of 100,000 at  $m/z = 400$ . The instrument is  
163 equipped with a nano-DESI source assembled from two fused-silica capillaries (150  $\mu\text{m}$  o.d./50  
164  $\mu\text{m}$  i.d.) (Roach et al., 2010b). Analyte molecules extracted into the liquid bridge formed  
165 between the two capillaries are transferred to a mass spectrometer inlet and ionized by  
166 nanoelectrospray. The analysis was performed under the following conditions: spray voltage of  
167 3-5 kV, 0.5-1 mm distance from the tip of the nanospray capillary to the 300 °C heated inlet of  
168 the LTQ-Orbitrap, and 0.3-0.9  $\mu\text{L}/\text{min}$  flow rate of acetonitrile : water (1:1 volume) solvent. The  
169 instrument was calibrated using a standard mixture of caffeine, MRFA (met-arg-phe-ala) peptide,  
170 and Ultramark 1621 (Thermo Scientific, Inc.) for the positive ion mode and a standard mixture  
171 containing sodium dodecyl sulfate, sodium taurocholate, and Ultramark 1621 (Thermo Scientific,  
172 Inc.) for the negative ion mode. Both positive and negative mode mass spectra were acquired  
173 using the Xcalibur software (Thermo Electron, Inc.). To analyze a sample, the nano-DESI probe  
174 was first placed on a clean area of the filter to record the background signal for  $\sim 3\text{min}$  and then  
175 positioned on the sample region to acquire data for an additional 4-5min (Roach et al., 2010a).

176 Peaks with  $S/N > 10$  were selected using the Decon2LS software developed at the Pacific  
177 Northwest National Laboratory (PNNL) (Jaitly et al., 2009). Further data processing was



178 performed with Microsoft Excel using a set of built-in macros developed by Roach et al. (2011).  
179 The background and sample peaks were aligned, and the peaks corresponding to  $^{13}\text{C}$  isotopes  
180 were removed. Only peaks in the sample spectra that are at least 10 times bigger than the  
181 corresponding peaks in the background spectra were retained for further analysis. Peaks were  
182 segregated into different groups using the higher-order mass defect transformation developed by  
183 Roach et al. (2011). Specifically, the peaks were first grouped using a  $\text{CH}_2$ -based transformation  
184 and then an  $\text{H}_2$ -based second-order transformation. Formula Calculator v. 1.1  
185 ([http://www.magnet.fsu.edu/usershub/scientificdivisions/icr/icr\\_software.html](http://www.magnet.fsu.edu/usershub/scientificdivisions/icr/icr_software.html)) was then used to  
186 assign the molecular formula to each group using the following constraints:  $\text{C} \geq 0$ ,  $\text{H} \geq 0$ ,  $\text{O} \geq 0$   
187 for the negative ion mode data and  $\text{C} \geq 0$ ,  $\text{H} \geq 0$ ,  $\text{O} \geq 0$ ,  $\text{Na} \leq 1$  for the positive ion mode data.  
188 Approximately 70% of the peaks were assigned with molecular formula within these constraints.  
189 The formulas of neutral species were subsequently determined by removing the adduct ion (e.g.,  
190 a proton or a sodium ion) from the positive ions or by adding a proton to the negative ions.

191 Kendrick representation of high resolution mass spectral data can be used to search for  
192 potential oligomeric units (Hughey et al., 2001). In this study, O-based Kendrick diagram was  
193 used to investigate the degree of hydroxylation. The Kendrick mass (KM) and Kendrick mass  
194 defect (KMD) are calculated using the following two equations:

$$195 \quad \text{KM} = \text{observed mass} \times 16 / 15.9949 \quad (1)$$

$$196 \quad \text{KMD} = \text{NM} - \text{KM} \quad (2)$$

197 Where, 16 is the nominal mass of O, 15.9949 is the exact mass of the O, and NM is the KM  
198 rounded to the nearest integer. Plotting KMD versus KM reveals homologous series of  
199 compounds differing only by the number of base units which fall on horizontal lines.

200 Double bond equivalent (DBE) indicates the number of double bonds and rings in a  
201 closed-shell organic molecule (Pellegrin, 1983). For a molecule with a nominal formula of  
202  $C_xH_yO_z$  (where  $x$ ,  $y$ ,  $z$  denote the number of C, H, and O atoms, respectively, in the molecule),  
203  $DBE = 1 - y/2 + x$ .

### 204 *2.2.3 Ion Chromatography (IC) and Total Organic Carbon (TOC) analysis*

205 Concentrations of inorganic/organic anions were measured using an ion chromatograph  
206 (Metrohm 881 Compact IC Pro, Switzerland) equipped with an autosampler, a Metrosep RP2  
207 guard/3.6 column and a Metrosep A Supp15 250/4.0 column, and a conductivity detector. Details  
208 on the IC method are given in Ge et al. (2014). Briefly, anions were eluted at 0.8 ml/min using  
209 an eluent of 5 mmol L<sup>-1</sup> Na<sub>2</sub>CO<sub>3</sub> and 0.3 mmol L<sup>-1</sup> NaOH in water. This method can separate and  
210 quantify 9 organic anions (glycolate, formate, acetate, pyruvate, oxalate, malate, malonate,  
211 maleate, and fumarate) and 7 inorganic anions (F<sup>-</sup>, Cl<sup>-</sup>, NO<sub>2</sub><sup>-</sup>, Br<sup>-</sup>, NO<sub>3</sub><sup>-</sup>, SO<sub>4</sub><sup>2-</sup> and PO<sub>4</sub><sup>3-</sup>). The IC  
212 results were evaluated in terms of reproducibilities of retention times and peak heights and  
213 linearity of the calibration curves. Analysis of external check standards, including a 7-anion  
214 standard mixture (Dionex) and 4 individual standards (Metrohm), always produced results that  
215 were within 10% of certified values. Relative differences for replicate analyses were within 3%.

216 A Shimadzu TOC-VCPH analyzer was applied to measure TOC in the aqSOA samples.  
217 The instrument uses a combustion tube filled with oxidation catalyst to convert all carbon atoms  
218 into CO<sub>2</sub> at 720 °C under ultrapure air and quantifies the resulting CO<sub>2</sub> using a non-dispersive  
219 infrared (NDIR) analyzer. Prior to combustion, inorganic carbon species  
220 (carbonates/bicarbonates and dissolved CO<sub>2</sub>) is transformed into CO<sub>2</sub> by 25% H<sub>3</sub>PO<sub>4</sub>, bubbled  
221 out, and determined by NDIR. TOC is determined as the difference. The TOC analyzer was  
222 calibrated using the standard solutions of NaHCO<sub>3</sub>, Na<sub>2</sub>CO<sub>3</sub>, and potassium hydrogen phthalate

223 (Sigma-Aldrich or Wako-Japan,  $\geq 99.0\%$ ). Results from external TOC check standards (Aqua  
224 Solutions) were always within 10% of certified values.

### 225 **3. Results and discussion**

#### 226 *3.1 Overview of the chemical characteristics of phenolic aqSOA*

227 The lifetime of phenols with respect to  $^3\text{C}^*$  and  $\bullet\text{OH}$  reactions in atmospheric fog and  
228 cloud water is on the order of minutes to hours during daytime (Smith et al., 2014). Compared to  
229  $\bullet\text{OH}$ ,  $^3\text{C}^*$  reacts more quickly with phenols, but the mass yields of aqSOA from both reactions  
230 are near 100% for phenol, guaiacol, and syringol (Smith et al., 2014). The reaction rate  
231 comparisons in this manuscript are based on the experimentally measured pseudo first-order rate  
232 constants for phenol loss ( $k'_{\text{ArOH}}$ ), which are equal to the product of the bimolecular rate constant  
233 and steady state concentration of oxidant:  $k'_{\text{ArOH}} = k_{\text{ArOH}+\text{Oxidant}}[\text{Oxidant}]$  (Smith et al., 2014).  
234 Based on bimolecular rate constants determined by Smith et al. (in preparation), the steady-state  
235 concentrations of  $\bullet\text{OH}$  and  $^3\text{C}^*$  during this study are estimated at  $10^{-16} \sim 10^{-15} \text{ mol L}^{-1}$  and  $\sim 10^{-14}$   
236  $\text{mol L}^{-1}$ , respectively, which are similar to the typical aqueous  $\bullet\text{OH}$  concentration in fog and  
237 cloud waters (Anastasio and McGregor, 2001; Arakaki et al., 2013) and the  $^3\text{C}^*$  concentration  
238 measured in Davis fog waters (R. Kaur, unpublished results).

239 As shown in Fig. 1 and summarized in Table 1, the aqSOA formed from all three phenols  
240 with both oxidants are highly oxygenated, with average O/C ratios in the range of 0.85-1.23 and  
241 average organic mass to carbon ratios (OM/OC) in the range of 2.27-2.79. Based on a  
242 comparison to the OM/OC of the precursors, the mass yields of the aqSOA should be 142 -  
243 214%, assuming all reacted phenols were converted into low volatility species. However, the  
244 measured values are 16-38% lower, indicating that approximately 16-38% of the reacted phenols  
245 were converted into volatile and semi-volatile species that evaporated during illumination and/or

246 drying. These results are consistent with a previous study by Sun et al. (2010), where O/C ratios  
247 of phenolic aqSOA formed from direct photodegradation and  $\bullet$ OH oxidation were in the range of  
248 0.80-1.06. The O/C of phenolic SOA from gas-phase  $\bullet$ OH oxidation are also near unity (Chhabra  
249 et al., 2011; Yee et al., 2013). Due to high oxygen contents, the organic mass-to-carbon (OM/OC)  
250 ratios of the aqSOA are high (average = 2.27-2.79; Table 1). Note that the OM/OC ratios  
251 determined by AMS agree well with those determined based on aqSOA mass measured  
252 gravimetrically and organic carbon mass measured by a TOC analyzer (Fig. S2). For the same  
253 oxidant, the O/C ratio of the aqSOA formed at  $t_{1/2}$  follows the order: phenol > guaiacol >  
254 syringol (Table 1). This trend is likely driven by precursor reactivity, which determines how long  
255 the solution needed to be illuminated to reach one half-life, and has the order: syringol >  
256 guaiacol > phenol. The reactivity differences among the three precursors are likely due to the  
257 electron-donating effect of the o-methoxy substituents, which may increase the rate of  
258 electrophilic reactions on the benzene ring. Longer illumination time increases the formation of  
259 highly oxygenated species and ring-opening species ( $n_C < 6$ ). For the same reason,  $\bullet$ OH oxidation,  
260 which is slower than  $^3C^*$  reaction for the same phenol precursor, generally produces more  
261 oxidized aqSOA at  $t_{1/2}$ .

262 Figures S3 and S4 show the nano-DESI MS spectra of the aqSOA of syringol, guaiacol,  
263 and phenol formed from  $^3C^*$  and  $\bullet$ OH reactions, respectively. Hundreds of species were  
264 identified, all of which are oxygenated with the median O/C ratios of the molecules varying from  
265 0.33-0.55 in different aqSOA samples (Fig. 1). The signal-weighted average O/C ratios  
266 (Bateman et al., 2012) of phenolic aqSOA are in the range of 0.31-0.65 according to the negative  
267 ion mode nano-DESI results, which are systematically lower than the average O/C of bulk  
268 aqSOA measured by the AMS (Fig. 1). However, due to large differences between the AMS and

269 the nano-DESI methodology, in terms of sample analysis, data processing, and assumptions used  
270 for average O/C calculations, a direct comparison between these two sets of O/C data should be  
271 cautioned.

272 Figure 2 shows the AMS spectra of different aqSOA acquired after 50% of the initial  
273 phenols had reacted (i.e., at  $t_{1/2}$ ). A prominent feature of these spectra is that  $\text{CO}_2^+$  ( $m/z = 44$ ),  
274  $\text{H}_2\text{O}^+$  ( $m/z = 18$ ), and  $\text{CO}^+$  ( $m/z = 28$ ) are the largest peaks, similar to the spectral pattern of fulvic  
275 acid – a model compound representative of highly processed and oxidized organic particulate  
276 matter and humic-like substances (HULIS) (Zhang et al., 2005; Ofner et al., 2011). The AMS  
277 spectra of syringol aqSOA formed from different oxidants are almost identical (Fig. 2),  
278 indicating similar chemical compositions. Similarly, nano-DESI analysis shows the formation of  
279 a large number of common species, i.e., 883 species with common elemental composition (Table  
280 1), through the reactions of syringol with  $^3\text{C}^*$  and  $\bullet\text{OH}$ , which account for 76% and 88%,  
281 respectively, of the total number of molecules identified in the corresponding aqSOA. A similar  
282 overlap of common species was observed for guaiacol aqSOA. But the molecular compositions  
283 of phenol aqSOA are more different between the two oxidants (Table 1), which is consistent with  
284 the fact that the AMS spectra of the two phenol aqSOA are largely different at  $m/z \geq 80$  (Fig. 2I).  
285 The more distinct compositional differences of phenol aqSOA between the  $\bullet\text{OH}$  and  $^3\text{C}^*$   
286 reactions is probably due to the larger difference in reaction times (i.e.,  $t_{1/2} = 672$  min vs. 480  
287 min; Table 1). Detailed discussions on the comparisons of aqSOA produced from the same  
288 precursor but different oxidants are given in Sect. 3.3.

289 A total number of 149 common molecules were identified in all samples (Table 1).  
290 Figure 3 shows the Van Krevelen diagram of these common molecules. A majority of these  
291 molecules have molecular weight lower than 400 Da and DBE < 12 (Fig. 3), indicating that they

292 contain two or less aromatic rings and that they were likely produced from ring-opening  
293 reactions. In addition, small carboxylate anions were observed in all aqSOA samples, although  
294 they represent only a small fraction of the TOC (Table 1). It is interesting to point out that the  
295 number of molecules observed by nano-DESI decreases with increasing illumination time across  
296 all 3 phenols, suggesting that increased aging simplifies the products to a smaller set (Table 1).  
297 However, this trend could also be related to ionization efficiency of different types of phenolic  
298 aqSOA. For example, syringol aqSOA has more methoxy groups, thus is easier to get ionized by  
299 nano-DESI, compared to phenol aqSOA.

300 Both flash-frozen (FF) and blown-down (BD) samples were chemically characterized and  
301 show almost identical AMS spectra (Fig. S5). We also found that the ESI-MS spectra of the  
302 aqueous solution of the blown-down sample and the flash-frozen sample for the aqSOA formed  
303 from syringol +  $^{13}\text{C}^*$  are also overall similar. These observations confirm that the non-volatile  
304 components of these two sample types are chemically very similar, and the blown-down  
305 procedure had relatively small influence on the observed product distribution. Since FF samples  
306 contain dissolved volatile species which should have evaporated during nebulization and drying,  
307 we estimated the amount of these species by examining the differences in the TOC  
308 concentrations between FF and BD samples after correction for the mass of unreacted precursors.  
309 Figure 4 shows the contributions of reactants (phenolic precursor and DMB) and products  
310 (dissolved volatile species and aqSOA) to the solution TOC after illumination to  $t_{1/2}$ . Dissolved  
311 volatile species formed during photolysis represent a small fraction (2.7 - 6.6%; Table 1) of the  
312 total carbon originally present in the reactants, consistent with the high mass yields of phenolic  
313 aqSOA reported by Smith et al. (2014).

### 314 *3.2 Insights into aqSOA formation mechanisms*

315 In this section we synthesize the molecular composition and bulk chemistry results and  
316 interpret the formation mechanisms of phenolic aqSOA. A notable result is the large number of  
317 dimer and higher oligomers (up to hexamer) found in the aqSOA. As shown in Figures S3 and  
318 S4, the nano-DESI MS spectra of phenolic aqSOA contain clearly distinguished regions  
319 corresponding to monomers, dimers, trimers, tetramers, pentamers, and hexamers and their  
320 oxidation products. We therefore determine the distributions of phenolic aqSOA species based  
321 on the degree of oligomerization by summing signals in each region (Fig. 5). Oligomers and  
322 related derivative species clearly account for a significant fraction (24.2% - 92.6%) of the total  
323 signals in the nano-DESI spectra of all phenolic aqSOA. Substituted monomers and ring-opening  
324 species ( $n_C < 6$ ) are also present in all aqSOA and they are particularly abundant in that of phenol  
325 +  $\bullet$ OH.

326 Table 2 lists the 10 most abundant compounds identified in the aqSOA of syringol  
327 formed through reaction with  $\bullet$ OH or  $^3\text{C}^*$ . Among them 7 are common species, including  
328 syringol dimer ( $\text{C}_{16}\text{H}_{18}\text{O}_6$ ), hydroxylated syringol ( $\text{C}_8\text{H}_{10}\text{O}_5$ ), three dimer derivatives ( $\text{C}_{15}\text{H}_{14}\text{O}_6$ ,  
329  $\text{C}_{15}\text{H}_{16}\text{O}_6$  and  $\text{C}_{15}\text{H}_{16}\text{O}_9$ ), and two monomer derivatives ( $\text{C}_{15}\text{H}_{18}\text{O}_7$  and  $\text{C}_{12}\text{H}_{12}\text{O}_7$ ). Guaiacol  
330 aqSOA is also dominated by the dimer and related species whereas substituted monomers are  
331 more abundant in phenol aqSOA (Fig. 5). The presence of dimers and substituted monomers is  
332 also evident in the AMS spectra. As an example, Figure 6 shows the AMS spectra of phenol  
333 aqSOA along with the NIST mass spectra of possible products. The spectra of guaiacol and  
334 syringol aqSOA are shown in Figures S6 and S7. Note that the AMS spectrum of biphenyl-4,4'-  
335 diol – a substituted phenolic compound – is very similar to the NIST mass spectrum (Fig. S8),  
336 indicating the validity of interpreting the AMS spectra of phenolic aqSOA based on the NIST

337 spectra of possible products. The AMS spectra of phenol aqSOA show a prominent peak at  $m/z =$   
338 186 ( $C_{12}H_{10}O_2^+$ ), which is the molecular ion ( $M^+$ ) of phenol dimer (Fig. 6). Similarly, the  
339 molecular ion of guaiacol dimer ( $C_{14}H_{14}O_4^+$ ;  $m/z = 246$ ; Fig. S6) is also noticeable in the AMS  
340 spectra. These results indicate that oligomerization is an important aqueous-phase reaction  
341 pathway that leads to the formation of aqSOA from phenols.

342 Hydroxylation is another important reaction pathway that forms and transforms phenolic  
343 aqSOA. As shown in Figure S9, the O-based Kendrick diagram of syringol aqSOA clearly  
344 indicates the presence of a large number of species with different degrees of hydroxylation.  
345 Similarly, AMS analysis reveals the ubiquitous formation of hydroxylated products as well. For  
346 example, the AMS spectra of phenol aqSOA show prominent peaks at  $m/z = 110$  ( $C_6H_6O_2^+$ ) and  
347  $m/z = 202$  ( $C_{12}H_{10}O_3^+$ ), suggesting the presence of hydroxylated phenol and hydroxylated phenol  
348 dimer, respectively (Fig. 6). In addition, signature ions representing 2-methoxyhydroquinone are  
349 detected in guaiacol aqSOA (Fig. S6) and 3,4,5-trihydroxy benzoic acid is likely a product of  
350 syringol oxidation (Fig. S7)

351 Both nano-DESI and AMS results further reveal the broad formation of aldehydes, esters,  
352 and carboxylated products. As shown in Table 2,  $C_9H_{10}O_4$  (MW = 182; DBE = 5), which was  
353 found to present at high abundance in the aqSOA of syringol +  $^3C^*$ , is likely a syringol aldehyde.  
354 In addition, the pronounced  $C_7H_5O_2^+$  ( $m/z = 121$ ) peak in the AMS spectra of phenol aqSOA (Fig.  
355 6a) indicates the formation of phenol esters such as methylparaben and ethylparaben (Fig. 6d)  
356 and the prominent  $C_8H_7O_3^+$  ( $m/z = 151$ ) signal in the guaiacol aqSOA spectra (Fig. S6a) suggests  
357 the formation of a guaiacol ester – methyl vanillate (Fig. S6c).

358 Small organic acid anions (i.e., formate, acetate, oxalate, malate, malonate, etc.) are  
359 observed in all samples and these species together account for less than 4% of the TOC in



360 aqSOA (Table 1). Note that the importance of organic acids is likely underestimated as IC only  
361 quantifies a limited number of low molecular weight aliphatic acids. Nano-DESI analysis further  
362 reveals the presence of a number of aromatic compounds with substituted carboxyl groups (e.g.,  
363 aromatic esters; Fig. S10) and the formation of highly oxygenated C3-C5 aliphatic species in all  
364 samples, some of which (e.g.,  $C_3H_4O_4$ ,  $C_4H_6O_4$  and  $C_5H_6O_5$ ) are likely carboxylic acids based on  
365 DBE values. Furthermore, both nano-DESI and AMS analyses identify demethoxylated aromatic  
366 products (e.g.,  $C_{15}H_{16}O_6$  and  $C_{15}H_{16}O_9$  in Table 2). These results together indicate that various  
367 fragmentation pathways, such as the cleavage of the aromatic rings and the losses of methoxy (-  
368  $OCH_3$ ) groups, are important during the aqueous-phase reactions of phenols.

369         Based on these results, we propose a scheme in Fig. 7 of the main pathways of aqSOA  
370 formation through the reactions of phenols +  $^3C^*$ . Briefly, phenols react with  $^3C^*$  and undergo  
371 multiple steps to form HOOH (Anastasio et al., 1997), which is a source of  $\bullet OH$  via photolysis.  
372 The addition of  $\bullet OH$  to the aromatic ring, followed by  $O_2$  addition and  $HO_2\bullet$  elimination, leads to  
373 the formation of hydroxylated products (Barzaghi and Herrmann, 2002). In the meantime, the  
374  $\bullet OH$ -phenol adduct can undergo unimolecular elimination of  $H_2O$  to form a phenoxy radical  
375 (Atkinson et al., 1992; Barzaghi and Herrmann, 2002; Olariu et al., 2002), which then combines  
376 with another radical to form dimer and higher oligomers. Note that the amount of HOOH  
377 produced in the reactions of phenols +  $^3C^*$  is small and  $\bullet OH$  oxidation appears to be negligible  
378 compared to the oxidation of phenols by  $^3C^*$  (Smith et al., 2014). Phenoxy radical may also form  
379 from the oxidation of phenols by  $^3C^*$  via electron transfer coupled with proton transfer from the  
380 phenoxy radical cation or from solvent water (Anastasio et al., 1997). Demethoxylation takes  
381 place through attachment of  $\bullet OH$  to ring positions occupied by methoxyl groups, followed by  
382 elimination of a methanol molecule to form semiquinone radicals (Steenken and O'Neill, 1977).

383 Esterification of phenols occurs through the reactions with organic acids (Offenhauer, 1964).  
384 Furthermore, the reactants and the products from all these pathways may undergo ring-opening  
385 process, forming ketones and carboxylic acids. Similar species, including oligomers, esters,  
386 carbonyls, carboxylic acids, and demethoxylated products, can be formed in  $\bullet\text{OH}$ -mediated  
387 reactions as well (Sun et al., 2010), although apparently with different reaction yields and rates.

### 388 ***3.3 Comparisons of phenolic aqSOA produced from different oxidants: $\bullet\text{OH}$ vs. $^3\text{C}^*$***

389 As discussed above, aqueous reactions of phenols produce a variety of low-volatility  
390 species including oligomers, functionalized monomer and oligomers (with varying numbers of  
391 carbonyl, carboxyl, ester, and hydroxyl groups), and small organic acids (e.g., formate, acetate,  
392 oxalate, and malate). Although aqSOA formed from the same precursor generally appear to be  
393 chemically similar, there are significant compositional differences between the products from  
394  $\bullet\text{OH}$  and  $^3\text{C}^*$  reactions. Overall, the molecular compositions of guaiacol and phenol aqSOA are  
395 more dependent on the oxidant than are syringol aqSOA (Fig. 5). Similarly, the AMS spectral  
396 patterns at  $m/z \geq 80$  exhibit more significant differences between  $\bullet\text{OH}$  and  $^3\text{C}^*$  for guaiacol ( $r^2 =$   
397  $0.65$ ; Fig. 2j) and phenol ( $r^2 = 0.42$ ; Fig. 2l) whereas those for syringol are almost identical ( $r^2 =$   
398  $0.97$ ; Fig. 2h). Furthermore, a majority of the aqSOA molecules of phenol +  $\bullet\text{OH}$  contain only  
399 one benzene ring, whereas the  $^3\text{C}^*$  reaction produces more oligomers and substituted species  
400 based on the DBE values.

401 Since the fragmentation pattern from 70 eV electron ionization is reproducible  
402 (McLafferty and Turecek, 1993), unique ions can be used as tracer species to quantify the  
403 concentration of the parent compound. Thus, we further compare the relative abundances of  
404 signature ions in the AMS spectra of the aqSOA formed from  $\bullet\text{OH}$ - and  $^3\text{C}^*$ -mediated reactions  
405 (Fig. 8). Details on the signature ions and their proposed precursors are given in Table S1. All

406 these ions are odd electron ions, which usually have special mechanistic significances and are  
407 more indicative of the chemical identities of the precursors (McLafferty and Turecek, 1993).  
408 These ions can potentially be used to analyze ambient organic aerosol data for the presence of  
409 phenolic aqSOA. For instance, a previous study by our group observed  $C_{16}H_{18}O_6^+$  ( $m/z$  306) and  
410  $C_{14}H_{14}O_4^+$  ( $m/z$  246) – signature ions representing syringol and guaiacol dimers, respectively, in  
411 ambient aerosols significantly influenced by wood combustion and fog processing (Sun et al.,  
412 2010). Similar to the nano-DESI results, the AMS results also indicate that the aqSOA formed  
413 via  $^3C^*$  are more enriched of dimers and higher oligomers compared to  $\bullet OH$  for a given phenol.  
414 These observations suggest that more coupling of phenoxy radicals takes place during reactions  
415 initiated by  $^3C^*$  than by  $\bullet OH$ . On the other hand, both IC and nano-DESI results indicate that  
416  $\bullet OH$ -mediated reactions promote the formation of organic acids and other ring-opening species  
417 ( $n_C < 6$ ) (see Sect. 3.2), consistent with the observations that  $\bullet OH$  reaction generally leads to  
418 more oxidized aqSOA as well as water-soluble volatile species (Table 1).

419 A possible reason for the compositional differences observed in the aqSOA of the same  
420 precursor but different oxidants is that  $^3C^*$  reacts faster with phenols (Smith et al., 2014) and  
421 thus takes shorter time to oxidize the same amount of phenols compared to  $\bullet OH$ . Longer  
422 illumination allows further oxidation and fragmentation of higher molecular weight species to  
423 happen, leading to the formation of smaller molecules with fewer aromatic rings. Indeed, the  
424 compositions of syringol aqSOA, which were produced after comparable illumination durations,  
425 are highly similar between the two oxidation conditions according to both nano-DESI and AMS  
426 results whereas the difference is the largest for phenol aqSOA whose illumination times are  
427 substantially different between  $^3C^*$  and  $\bullet OH$  oxidation (Figs. 2 and 5). However, the fact that  
428 there are more oligomers and their derivatives in guaiacol +  $^3C^*$  condition compared to syringol

429 + •OH (Fig. 5) even though the illumination durations are similar (Table 1) suggests that  
430 coupling of phenoxy radicals is a more favored pathway through  $^3\text{C}^*$  reaction.

### 431 *3.4 Volatility profiles and UV-vis absorption spectra of phenolic aqSOA*

432 As discussed above, the chemical compositions of phenolic aqSOA are complex. As a  
433 result, the volatilities of the aqSOA species span a broad range, from very low vapor pressure  
434 compounds such as oligomers to more volatile species such as low molecular weight acids.  
435 Figure 9 shows the volatility profiles of phenolic aqSOA formed from  $^3\text{C}^*$  reactions measured by  
436 a thermodenuder coupled with the AMS. Ammonium sulfate and ammonium nitrate were  
437 analyzed simultaneously as references. On average, phenolic aqSOA are more volatile than  
438 ammonium sulfate, but less volatile than ammonium nitrate (Fig. 9). The fact that a significant  
439 fraction of the aqSOA mass remains in the particle phase even at 200 °C (Fig. 9) is consistent  
440 with the presence of some very low volatility species such as oligomers. Compared to guaiacol  
441 and syringol aqSOA, phenol aqSOA show the slowest decay with increasing TD temperature,  
442 indicating that they are comprised of more low-volatility species. This is consistent with our  
443 chemical analyses which reveal that the aqSOA of phenol +  $^3\text{C}^*$  are composed of a larger  
444 fraction of species containing more than two aromatic rings, including trimer and higher  
445 oligomers (Fig. 5). This is also consistent with fact that the O/C ratios of phenol aqSOA are  
446 highest among all three precursors for the same oxidant. These results together suggest that the  
447 volatility of phenolic aqSOA is strongly influenced by both polymer contents and average  
448 oxidation degree, as reported previously (Huffman et al., 2009).

449 Recently, light-absorbing OA, also termed “brown carbon”, has attracted much attention,  
450 due to their ability to absorb sunlight and thus affect the radiative budget of the earth (Shapiro et  
451 al., 2009). Previous studies have shown that the aqueous-phase oxidation of phenols forms low-

452 volatility oligomers, which absorb significant amounts of UV-visible light and likely account for  
453 a significant portion of atmospheric HULIS (Gelencser et al., 2003; Chang and Thompson, 2010).  
454 In this study, we examined the optical properties of phenolic aqSOA using UV-vis spectroscopy.  
455 Figure 10 shows an example of the UV-vis spectra of syringol aqSOA formed in the reactions  
456 with  $^3\text{C}^*$  and  $\bullet\text{OH}$ , respectively, at  $t_{1/2}$ . Both syringol aqSOA samples absorb in the tropospheric  
457 sunlight wavelengths ( $> 300$  nm), while syringol does not. This enhancement is likely explained  
458 by the formation of conjugated structures as a result of polymerization and functionalization due  
459 to the additions of hydroxyl, carbonyl, and carboxyl functional groups to the aromatic rings.  
460 Phenol and guaiacol aqSOA also show enhanced absorption in the tropospheric sunlight  
461 wavelengths ( $> 300$  nm), while phenol and guaiacol themselves do not. These results indicate  
462 that aqueous-phase reactions of phenols are likely an important source of brown carbon in the  
463 atmosphere, especially in regions influenced by biomass burning.

#### 464 **4. Conclusions and implications**

465 We thoroughly characterized the chemical composition and studied the volatility and  
466 optical properties of phenolic aqSOA formed via reactions with two different oxidants:  $^3\text{C}^*$  and  
467  $\bullet\text{OH}$ . Elemental analysis of the AMS spectra indicates that all phenolic aqSOA are highly  
468 oxidized (O/C ratios: 0.85-1.23), despite the fact that some of the reactions were very fast ( $t_{1/2} <$   
469 1 hr for syringol). For the same oxidant, the oxidation degree of the aqSOA formed at  $t_{1/2}$  follows  
470 the order: phenol  $>$  guaiacol  $>$  syringol. A large number of aqSOA molecules are identified,  
471 including oligomers (up to hexamers) and their derivatives with varying numbers of carbonyl,  
472 carboxyl, ester, and hydroxyl groups. A large number of ring-opening species ( $n_{\text{C}} < 6$ ) including  
473 small organic acids (e.g., oxalate, formate, and acetate) are also identified. While the bulk  
474 compositions of the aqSOA are overall similar at  $t_{1/2}$  between the two oxidants for a given

475 precursor, compositional differences are observed. Generally speaking, reactions mediated by  
476 •OH produce more highly oxygenated species with a single aromatic ring, while oxidation by  
477  $^3\text{C}^*$  enhances the formation of higher molecular weight species including oligomers and their  
478 oxygenated derivatives. The physical properties, such as volatility and light absorptivity, of the  
479 phenol aqSOA depend on their chemical compositions. Our thermodenuder experiments indicate  
480 that the volatility profiles of phenolic aqSOA are influenced by both oligomer contents and  
481 average oxidation degree. In addition, the formation of aqSOA species with enhanced conjugated  
482 double bonds is probably responsible for the significant light absorption in the actinic region,  
483 suggesting that aqueous-phase reactions of phenols are an important source of brown carbon in  
484 the atmosphere.

485 Overall, our results indicate that aqueous-phase processing of phenols represents an  
486 important pathway for the production of low-volatility, highly oxygenated and high molecular  
487 weight species, which remain in the particle phase after water evaporation. Since phenolic  
488 aqSOA is both water soluble and light absorbing, understanding the impacts of these reactions on  
489 the chemical and physical properties, and thus the climatic and health effects, of atmospheric  
490 particles may be important, especially in regions influenced by biomass burning emissions. An  
491 approach for evaluating the importance of phenolic aqSOA formation in the atmosphere is to  
492 systematically analyze the AMS mass spectra of ambient aerosol for signature ions  
493 representative of phenolic aqSOA. AMS has been broadly applied for chemical analysis of  
494 ambient aerosol and multivariate statistical approaches (e.g., positive matrix factorization) have  
495 been frequently used on organic aerosol mass spectral data to determine factors representing  
496 different sources and processes (Ulbrich et al., 2009; Zhang et al., 2011). An important criterion  
497 for validating the extracted factor is via examining the mass spectra of the factors for signature

498 ions (Zhang et al., 2011). The fact that AMS uses 70 eV EI ionization, which ionizes and  
499 fragments molecules with reproducible pattern (McLafferty and Turecek, 1993), allows for the  
500 identification and quantification of certain compounds or compound classes in a mixture via  
501 signature ions. Indeed, previous studies have demonstrated the capability of using unique AMS  
502 ions to fingerprint species such as hydrocarbon-like and oxygenated organic aerosols (Zhang et  
503 al., 2005), polycyclic aromatic hydrocarbons (PAH) (Dzepina et al., 2007), methanesulfonic acid  
504 (MSA) (Ge et al., 2012), and certain nitrogen- and sulfur-containing organic aerosols (Farmer et  
505 al., 2010; Ge et al., 2014).

506 With this in mind, this study suggests several ions that are potentially representative of  
507 phenolic aqSOA, including  $C_{16}H_{18}O_6^+$  ( $m/z = 306$ ) for syringol dimer,  $C_{14}H_{14}O_4^+$  ( $m/z = 246$ ) for  
508 guaiacol dimer,  $C_{14}H_{14}O_5^+$  ( $m/z = 262$ ) and  $C_{14}H_{14}O_6^+$  ( $m/z = 278$ ) for hydroxylated guaiacol  
509 dimer,  $C_{12}H_{10}O_2^+$  ( $m/z = 186$ ) for phenol dimer,  $C_{21}H_{20}O_6^+$  ( $m/z = 368$ ) for guaiacol trimer, and  
510  $C_{18}H_{14}O_3^+$  ( $m/z = 278$ ) for phenol trimer (Fig. 8). Since all these ions have odd number of  
511 electrons with relatively high  $m/z$ 's, their productions in the AMS are more directly linked to the  
512 specific parent compounds, meaning that they are less likely contributed by confounding  
513 molecules (McLafferty and Turecek, 1993). In addition, while large hydrocarbon molecules, e.g.,  
514 those from vehicle emissions, may generate significant ion signals at  $m/z > 200$ , most of them are  
515 even-electron ions and contain no oxygen. They are therefore easily differentiated from the  
516 isobaric ions from phenolic SOA. Nevertheless, it is important to point out that the validity of  
517 using the aqSOA signature ions identified in this study needs to be evaluated by examining  
518 ambient organic aerosol mass spectrometry data. In addition, analyzing field samples with nano-  
519 DESI may also provide important insights into the impacts of aqueous phase processing of  
520 phenolic compounds in the atmosphere.

## 521 **Acknowledgements**

522 This work was supported by the U.S. National Science Foundation, Grant No. AGS-  
523 1036675 and the California Agricultural Experiment Station (Projects CA-D-ETX-2102-H and  
524 CA-D\*-LAW-6403-RR). The nano-DESI MS analysis was performed at the W.R. Wiley  
525 Environmental Molecular Sciences Laboratory (EMSL) - a national scientific user facility  
526 located at PNNL, and sponsored by the Office of Biological and Environmental Research of the  
527 U.S. PNNL is operated for US DOE by Battelle Memorial Institute under Contract No. DE-  
528 AC06-76RL0 1830. Additional funding was provided by a Jastro-Shields Graduate Research  
529 Award (UC Davis) and graduate fellowships from the Atmospheric Aerosols and Health (AAH)  
530 program at UC Davis to Lu Yu and Jeremy Smith. We thank Dr. Ann Dillner, Kathryn George,  
531 and Dr. Sonya Collier for help with experiments.

## 532 **References**

- 533 Aiken, A. C., Decarlo, P. F., Kroll, J. H., Worsnop, D. R., Huffman, J. A., Docherty, K. S.,  
534 Ulbrich, I. M., Mohr, C., Kimmel, J. R., Sueper, D., Sun, Y., Zhang, Q., Trimborn, A., Northway, M.,  
535 Ziemann, P. J., Canagaratna, M. R., Onasch, T. B., Alfarra, M. R., Prevot, A. S. H., Dommen, J.,  
536 Duplissy, J., Metzger, A., Baltensperger, U. and Jimenez, J. L.: O/C and OM/OC ratios of primary,  
537 secondary, and ambient organic aerosols with high-resolution time-of-flight aerosol mass spectrometry,  
538 *Environ. Sci. Technol.*, 42, 4478-4485, doi:10.1021/es703009q, 2008.
- 539 Allan, J. D., Delia, A. E., Coe, H., Bower, K. N., Alfarra, M. R., Jimenez, J. L., Middlebrook, A.  
540 M., Drewnick, F., Onasch, T. B., Canagaratna, M. R., Jayne, J. T. and Worsnop, D. R.: A generalised  
541 method for the extraction of chemically resolved mass spectra from Aerodyne aerosol mass spectrometer  
542 data, *J. Aerosol Sci.*, 35, 909-922, doi:10.1016/j.jaerosci.2004.02.007, 2004.
- 543 Altieri, K. E., Carlton, A. G., Lim, H. J., Turpin, B. J. and Seitzinger, S. P.: Evidence for  
544 oligomer formation in clouds: reactions of isoprene oxidation products, *Environ. Sci. Technol.*, 40, 4956-  
545 4960, doi:10.1021/es052170n, 2006.
- 546 Anastasio, C., Faust, B. C. and Rao, C. J.: Aromatic carbonyl compounds as aqueous-phase  
547 photochemical sources of hydrogen peroxide in acidic sulfate aerosols, fogs, and clouds .1. Non-phenolic  
548 methoxybenzaldehydes and methoxyacetophenones with reductants (phenols), *Environ. Sci. Technol.*, 31,  
549 218-232, doi:10.1021/es960359g, 1997.
- 550 Anastasio, C. and McGregor, K. G.: Chemistry of fog waters in California's Central Valley: 1. In  
551 situ photoformation of hydroxyl radical and singlet molecular oxygen, *Atmos. Environ.*, 35, 1079-1089,  
552 doi:10.1016/s1352-2310(00)00281-8, 2001.
- 553 Arakaki, T., Anastasio, C., Kuroki, Y., Nakajima, H., Okada, K., Kotani, Y., Handa, D., Azechi,  
554 S., Kimura, T., Tshako, A. and Miyagi, Y.: A General Scavenging Rate Constant for Reaction of  
555 Hydroxyl Radical with Organic Carbon in Atmospheric Waters, *Environ. Sci. Technol.*, 47, 8196-8203,  
556 doi:10.1021/es401927b, 2013.



557 Aregahegn, K. Z., Noziere, B. and George, C.: Organic aerosol formation photo-enhanced by the  
558 formation of secondary photosensitizers in aerosols, *Faraday Disc.*, 165, 123-134,  
559 doi:10.1039/C3FD00044C, 2013.

560 Atkinson, R., Aschmann, S. M. and Arey, J.: Reactions of hydroxyl and nitrogen trioxide radicals  
561 with phenol, cresols, and 2-nitrophenol at 296±2 K, *Environ. Sci. Technol.*, 26, 1397-1403,  
562 doi:10.1021/es00031a018, 1992.

563 Barzaghi, P. and Herrmann, H.: A mechanistic study of the oxidation of phenol by OH/NO<sub>2</sub>/NO<sub>3</sub>  
564 in aqueous solution, *Phys. Chem. Chem. Phys.*, 4, 3669-3675, doi:10.1039/b201652d, 2002.

565 Bateman, A. P., Laskin, J., Laskin, A. and Nizkorodov, S. A.: Applications of high-resolution  
566 electrospray ionization mass spectrometry to measurements of average oxygen to carbon ratios in  
567 secondary organic aerosols, *Environ. Sci. Technol.*, 46, 8315-8324, doi:10.1021/es3017254, 2012.

568 Blando, J. D. and Turpin, B. J.: Secondary organic aerosol formation in cloud and fog droplets: a  
569 literature evaluation of plausibility, *Atmos. Environ.*, 34, 1623-1632, doi:10.1016/S1352-2310(99)00392-  
570 1, 2000.

571 Canagaratna, M. R., Jayne, J. T., Jimenez, J. L., Allan, J. D., Alfarra, M. R., Zhang, Q., Onasch, T.  
572 B., Drewnick, F., Coe, H., Middlebrook, A., Delia, A., Williams, L. R., Trimborn, A. M., Northway, M. J.,  
573 DeCarlo, P. F., Kolb, C. E., Davidovits, P. and Worsnop, D. R.: Chemical and microphysical  
574 characterization of ambient aerosols with the aerodyne aerosol mass spectrometer, *Mass Spectrom. Rev.*,  
575 26, 185-222, doi:10.1002/mas.20115, 2007.

576 Canonica, S., Hellrung, B. and Wirz, J.: Oxidation of phenols by triplet aromatic ketones in  
577 aqueous solution, *J. Phys. Chem. A*, 104, 1226-1232, doi:10.1021/jp9930550, 2000.

578 Chang, J. L. and Thompson, J. E.: Characterization of colored products formed during irradiation  
579 of aqueous solutions containing H<sub>2</sub>O<sub>2</sub> and phenolic compounds, *Atmos. Environ.*, 44, 541-551,  
580 doi:10.1016/j.atmosenv.2009.10.042, 2010.

581 Chhabra, P. S., Ng, N. L., Canagaratna, M. R., Corrigan, A. L., Russell, L. M., Worsnop, D. R.,  
582 Flagan, R. C. and Seinfeld, J. H.: Elemental composition and oxidation of chamber organic aerosol,  
583 *Atmos. Chem. Phys.*, 11, 8827-8845, doi:10.5194/acp-11-8827-2011, 2011.

584 Collier, S. and Zhang, Q.: Gas-phase CO<sub>2</sub> subtraction for improved measurements of the organic  
585 aerosol mass concentration and oxidation degree by an aerosol mass spectrometer, *Environ. Sci. Technol.*,  
586 47, 14324-14331, doi:10.1021/es404024h, 2013.

587 DeCarlo, P. F., Kimmel, J. R., Trimborn, A., Northway, M. J., Jayne, J. T., Aiken, A. C., Gonin,  
588 M., Fuhrer, K., Horvath, T., Docherty, K. S., Worsnop, D. R. and Jimenez, J. L.: Field-deployable, high-  
589 resolution, time-of-flight aerosol mass spectrometer, *Anal. Chem.*, 78, 8281-8289,  
590 doi:10.1021/ac061249n, 2006.

591 Dzepina, K., Arey, J., Marr, L. C., Worsnop, D. R., Salcedo, D., Zhang, Q., Onasch, T. B.,  
592 Molina, L. T., Molina, M. J. and Jimenez, J. L.: Detection of particle-phase polycyclic aromatic  
593 hydrocarbons in Mexico City using an aerosol mass spectrometer, *Int. J. Mass Spectrom.*, 263, 152-170,  
594 doi:10.1016/j.ijms.2007.01.010, 2007.

595 Ervens, B., Turpin, B. J. and Weber, R. J.: Secondary organic aerosol formation in cloud droplets  
596 and aqueous particles (aqSOA): a review of laboratory, field and model studies, *Atmos. Chem. Phys.*, 11,  
597 11069-11102, doi:10.5194/acp-11-11069-2011, 2011.

598 Farmer, D. K., Matsunaga, A., Docherty, K. S., Surratt, J. D., Seinfeld, J. H., Ziemann, P. J. and  
599 Jimenez, J. L.: Response of an aerosol mass spectrometer to organonitrates and organosulfates and  
600 implications for atmospheric chemistry, *Proc. Natl. Acad. Sci.*, 107, 6670-6675,  
601 doi:10.1073/pnas.0912340107, 2010.

602 Fierz, M., Vernooij, M. G. C. and Burtscher, H.: An improved low-flow thermodenuder, *J.*  
603 *Aerosol Sci.*, 38, 1163-1168, doi:10.1016/j.jaerosci.2007.08.006, 2007.

604 Ge, X., Setyan, A., Sun, Y. and Zhang, Q.: Primary and secondary organic aerosols in Fresno,  
605 California during wintertime: Results from high resolution aerosol mass spectrometry, *J. Geophys. Res.*,  
606 117, D19301, doi:10.1029/2012JD018026, 2012.

607 Ge, X., Shaw, S. L. and Zhang, Q.: Toward understanding amines and their degradation products  
608 from postcombustion CO<sub>2</sub> capture processes with aerosol mass spectrometry, *Environ. Sci. Technol.*, 48,  
609 5066-5075, doi:10.1021/es4056966, 2014.

610 Gelencser, A., Hoffer, A., Kiss, G., Tombacz, E., Kurdi, R. and Bencze, L.: In-situ formation of  
611 light-absorbing organic matter in cloud water, *J. Atmos. Chem.*, 45, 25-33, doi:10.1023/a:1024060428172,  
612 2003.

613 George, K. M., Ruthenburg, T. C., Smith, J. D., Anastasio, C., Yu, L., Zhang, Q. and Dillner, A.:  
614 FT-IR quantification of the carbonyl functional group in aqueous-phase secondary organic aerosol from  
615 phenols, *Atmos. Environ.*, 2014.

616 Hallquist, M., Wenger, J. C., Baltensperger, U., Rudich, Y., Simpson, D., Claeys, M., Dommen,  
617 J., Donahue, N. M., George, C., Goldstein, A. H., Hamilton, J. F., Herrmann, H., Hoffmann, T., Iinuma,  
618 Y., Jang, M., Jenkin, M. E., Jimenez, J. L., Kiendler-Scharr, A., Maenhaut, W., McFiggans, G., Mentel, T.  
619 F., Monod, A., Prevot, A. S. H., Seinfeld, J. H., Surratt, J. D., Szmigielski, R. and Wildt, J.: The  
620 formation, properties and impact of secondary organic aerosol: current and emerging issues, *Atmos.*  
621 *Chem. Phys.*, 9, 5155-5236, doi:10.5194/acp-9-5155-2009, 2009.

622 Hawthorne, S. B., Krieger, M. S., Miller, D. J. and Mathiason, M. B.: Collection and quantitation  
623 of methoxylated phenol tracers for atmospheric-pollution from residential wood stoves, *Environ. Sci.*  
624 *Technol.*, 23, 470-475, doi:10.1021/es00181a013, 1989.

625 Hawthorne, S. B., Miller, D. J., Langenfeld, J. J. and Krieger, M. S.: PM-10 high-volume  
626 collection and quantitation of semi- and nonvolatile phenols, methoxylated phenols, alkanes, and  
627 polycyclic aromatic hydrocarbons from winter urban air and their relationship to wood smoke emissions,  
628 *Environ. Sci. Technol.*, 26, 2251-2262, doi:10.1021/es00035a026, 1992.

629 Huffman, J. A., Docherty, K. S., Mohr, C., Cubison, M. J., Ulbrich, I. M., Ziemann, P. J., Onasch,  
630 T. B. and Jimenez, J. L.: Chemically-resolved volatility measurements of organic aerosol from different  
631 sources, *Environ. Sci. Technol.*, 43, 5351-5357, doi:10.1021/es803539d, 2009.

632 Hughey, C. A., Hendrickson, C. L., Rodgers, R. P., Marshall, A. G. and Qian, K. N.: Kendrick  
633 mass defect spectrum: A compact visual analysis for ultrahigh-resolution broadband mass spectra, *Anal.*  
634 *Chem.*, 73, 4676-4681, doi:10.1021/ac010560w, 2001.

635 Jaitly, N., Mayampurath, A., Littlefield, K., Adkins, J. N., Anderson, G. A. and Smith, R. D.:  
636 Decon2LS: An open-source software package for automated processing and visualization of high  
637 resolution mass spectrometry data, *BMC Bioinformatics*, 10, 87, doi:10.1186/1471-2105-10-87, 2009.

638 Jimenez, J. L., Canagaratna, M. R., Donahue, N. M., Prevot, A. S. H., Zhang, Q., Kroll, J. H.,  
639 DeCarlo, P. F., Allan, J. D., Coe, H., Ng, N. L., Aiken, A. C., Docherty, K. S., Ulbrich, I. M., Grieshop, A.  
640 P., Robinson, A. L., Duplissy, J., Smith, J. D., Wilson, K. R., Lanz, V. A., Hueglin, C., Sun, Y. L., Tian,  
641 J., Laaksonen, A., Raatikainen, T., Rautiainen, J., Vaattovaara, P., Ehn, M., Kulmala, M., Tomlinson, J.  
642 M., Collins, D. R., Cubison, M. J., Dunlea, E. J., Huffman, J. A., Onasch, T. B., Alfarra, M. R., Williams,  
643 P. I., Bower, K., Kondo, Y., Schneider, J., Drewnick, F., Borrmann, S., Weimer, S., Demerjian, K.,  
644 Salcedo, D., Cottrell, L., Griffin, R., Takami, A., Miyoshi, T., Hatakeyama, S., Shimono, A., Sun, J. Y.,  
645 Zhang, Y. M., Dzepina, K., Kimmel, J. R., Sueper, D., Jayne, J. T., Herndon, S. C., Trimborn, A. M.,  
646 Williams, L. R., Wood, E. C., Middlebrook, A. M., Kolb, C. E., Baltensperger, U. and Worsnop, D. R.:  
647 Evolution of organic aerosols in the atmosphere, *Science*, 326, 1525-1529, doi:10.1126/science.1180353,  
648 2009.

649 Kanakidou, M., Seinfeld, J. H., Pandis, S. N., Barnes, I., Dentener, F. J., Facchini, M. C., Van  
650 Dingenen, R., Ervens, B., Nenes, A., Nielsen, C. J., Swietlicki, E., Putaud, J. P., Balkanski, Y., Fuzzi, S.,  
651 Horth, J., Moortgat, G. K., Winterhalter, R., Myhre, C. E. L., Tsigaridis, K., Vignati, E., Stephanou, E. G.  
652 and Wilson, J.: Organic aerosol and global climate modelling: a review, *Atmos. Chem. Phys.*, 5, 1053-  
653 1123, doi:10.5194/acp-5-1053-2005, 2005.

654 Krueve, A., Kaupmees, K., Liigand, J. and Leito, I.: Negative Electrospray Ionization via  
655 Deprotonation: Predicting the Ionization Efficiency, *Anal Chem*, 86, 4822-4830, doi:10.1021/ac404066v,  
656 2014.

657 Leuenberger, C., Ligocki, M. P. and Pankow, J. F.: Trace organic compounds in rain. 4. Identities,  
658 concentrations, and scavenging mechanisms for phenols in urban air and rain, *Environ. Sci. Technol.*, 19,  
659 1053-1058, doi:10.1021/es00141a005, 1985.

660 Lim, H. J., Carlton, A. G. and Turpin, B. J.: Isoprene forms secondary organic aerosol through  
661 cloud processing: Model simulations, *Environ. Sci. Technol.*, 39, 4441-4446, doi:10.1021/es048039h,  
662 2005.

663 McLafferty, F. W. and Turecek, F.: *Interpretation of Mass Spectra*, University Science Books,  
664 Mill Valley, California, 1993.

665 Monge, M. E., Rosenørn, T., Favez, O., Müller, M., Adler, G., Abo Riziq, A., Rudich, Y.,  
666 Herrmann, H., George, C. and D'Anna, B.: Alternative pathway for atmospheric particles growth, *Proc.*  
667 *Natl. Acad. Sci.*, 109, 6840-6844, doi:10.1073/pnas.1120593109, 2012.

668 Murphy, D. M., Cziczo, D. J., Froyd, K. D., Hudson, P. K., Matthew, B. M., Middlebrook, A. M.,  
669 Peltier, R. E., Sullivan, A., Thomson, D. S. and Weber, R. J.: Single-particle mass spectrometry of  
670 tropospheric aerosol particles, *J. Geophys. Res.-Atmos.*, 111, D23S32, doi:10.1029/2006jd007340, 2006.

671 Offenhauer, R. D.: The direct esterification of phenols, *J. Chem. Educ.*, 41, 39,  
672 doi:10.1021/ed041p39, 1964.

673 Ofner, J., Krüger, H. U., Grothe, H., Schmitt-Kopplin, P., Whitmore, K. and Zetzsch, C.:  
674 Physico-chemical characterization of SOA derived from catechol and guaiacol - a model substance for the  
675 aromatic fraction of atmospheric HULIS, *Atmos. Chem. Phys.*, 11, 1-15, doi:10.5194/acp-11-1-2011,  
676 2011.

677 Olariu, R. I., Klotz, B., Barnes, I., Becker, K. H. and Mocanu, R.: FT-IR study of the ring-  
678 retaining products from the reaction of OH radicals with phenol, o-, m-, and p-cresol, *Atmos. Environ.*, 36,  
679 3685-3697, doi:10.1016/s1352-2310(02)00202-9, 2002.

680 Pellegrin, V.: Molecular formulas of organic compounds: the nitrogen rule and degree of  
681 unsaturation, *J. Chem. Educ.*, 60, 626-633, doi:10.1021/ed060p626, 1983.

682 Roach, P. J., Laskin, J. and Laskin, A.: Molecular characterization of organic aerosols using  
683 nanospray-desorption/electrospray ionization-mass spectrometry, *Anal. Chem.*, 82, 7979-7986,  
684 doi:10.1021/ac101449p, 2010a.

685 Roach, P. J., Laskin, J. and Laskin, A.: Nanospray desorption electrospray ionization: an ambient  
686 method for liquid-extraction surface sampling in mass spectrometry, *Analyst*, 135, 2233-2236,  
687 doi:10.1039/c0an00312c, 2010b.

688 Roach, P. J., Laskin, J. and Laskin, A.: Higher-order mass defect analysis for mass spectra of  
689 complex organic mixtures, *Anal. Chem.*, 83, 4924-4929, doi:10.1021/ac200654j, 2011.

690 Rossignol, S., Aregahegn, K. Z., Tinel, L., Fine, L., Noziere, B. and George, C.: Glyoxal Induced  
691 Atmospheric Photosensitized Chemistry Leading to Organic Aerosol Growth, *Environ. Sci. Technol.*, 48,  
692 3218-3227, doi:10.1021/es405581g, 2014.

693 Sagebiel, J. C. and Seiber, J. N.: Studies on the occurrence and distribution of wood smoke  
694 marker compounds in foggy atmospheres, *Environ. Toxicol. Chem.*, 12, 813-822,  
695 doi:10.1002/etc.5620120504, 1993.

696 Sander, R.: *Compilation of Henry's Law constants for inorganic and organic species of potential*  
697 *importance in environmental chemistry*, available at: <http://irs.ub.rug.nl/dbi/4581696d8b3ed> (last access:  
698 14 December 2006), 1999.

699 Schauer, J. J., Kleeman, M. J., Cass, G. R. and Simoneit, B. R. T.: Measurement of emissions  
700 from air pollution sources. 3. C-1-C-29 organic compounds from fireplace combustion of wood, *Environ.*  
701 *Sci. Technol.*, 35, 1716-1728, doi:10.1021/es001331e, 2001.

702 Shapiro, E. L., Szprengiel, J., Sareen, N., Jen, C. N., Giordano, M. R. and McNeill, V. F.: Light-  
703 absorbing secondary organic material formed by glyoxal in aqueous aerosol mimics, *Atmos. Chem. Phys.*,  
704 9, 2289-2300, doi:10.5194/acp-9-2289-2009, 2009.

705 Simoneit, B. R. T., Schauer, J. J., Nolte, C. G., Oros, D. R., Elias, V. O., Fraser, M. P., Rogge, W.  
706 F. and Cass, G. R.: Levoglucosan, a tracer for cellulose in biomass burning and atmospheric particles,  
707 *Atmos. Environ.*, 33, 173-182, doi:10.1016/s1352-2310(98)00145-9, 1999.

708 Smith, J. D., Sio, V., Yu, L., Zhang, Q. and Anastasio, C.: Secondary organic aerosol production  
709 from aqueous reactions of atmospheric phenols with an organic triplet excited state, *Environ. Sci.*  
710 *Technol.*, 48, 1049-1057, doi:10.1021/es4045715, 2014.

711 Steenken, S. and O'Neill, P.: Oxidative demethoxylation of methoxylated phenols and  
712 hydroxybenzoic acids by the hydroxyl radical. An in situ electron spin resonance, conductometric pulse  
713 radiolysis and product analysis study, *J. Phys. Chem.*, 81, 505-508, doi:10.1021/j100521a002, 1977.

714 Sun, Y., Zhang, Q., Macdonald, A. M., Hayden, K., Li, S. M., Liggio, J., Liu, P. S. K., Anlauf, K.  
715 G., Leaitch, W. R., Steffen, A., Cubison, M., Worsnop, D. R., van Donkelaar, A. and Martin, R. V.: Size-  
716 resolved aerosol chemistry on Whistler Mountain, Canada with a high-resolution aerosol mass  
717 spectrometer during INTEX-B, *Atmos. Chem. Phys.*, 9, 3095-3111, doi:10.5194/acp-9-3095-2009, 2009.

718 Sun, Y. L., Zhang, Q., Anastasio, C. and Sun, J.: Insights into secondary organic aerosol formed  
719 via aqueous-phase reactions of phenolic compounds based on high resolution mass spectrometry, *Atmos.*  
720 *Chem. Phys.*, 10, 4809-4822, doi:10.5194/acp-10-4809-2010, 2010.

721 Ulbrich, I. M., Canagaratna, M. R., Zhang, Q., Worsnop, D. R. and Jimenez, J. L.: Interpretation  
722 of organic components from Positive Matrix Factorization of aerosol mass spectrometric data, *Atmos.*  
723 *Chem. Phys.*, 9, 2891-2918, doi:10.5194/acp-9-2891-2009, 2009.

724 Yee, L. D., Kautzman, K. E., Loza, C. L., Schilling, K. A., Coggon, M. M., Chhabra, P. S., Chan,  
725 M. N., Chan, A. W. H., Hersey, S. P., Crounse, J. D., Wennberg, P. O., Flagan, R. C. and Seinfeld, J. H.:  
726 Secondary organic aerosol formation from biomass burning intermediates: phenol and methoxyphenols,  
727 *Atmos. Chem. Phys.*, 13, 8019-8043, doi:10.5194/acp-13-8019-2013, 2013.

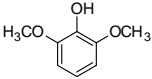
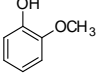
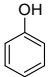
728 Zhang, Q., Alfarra, M. R., Worsnop, D. R., Allan, J. D., Coe, H., Canagaratna, M. R. and Jimenez,  
729 J. L.: Deconvolution and quantification of hydrocarbon-like and oxygenated organic aerosols based on  
730 aerosol mass spectrometry, *Environ. Sci. Technol.*, 39, 4938-4952, doi:10.1021/es048568l, 2005.

731 Zhang, Q., Jimenez, J., Canagaratna, M., Ulbrich, I., Ng, N., Worsnop, D. and Sun, Y.:  
732 Understanding atmospheric organic aerosols via factor analysis of aerosol mass spectrometry: a review,  
733 *Anal. Bioanal. Chem.*, 401, 3045-3067, doi:10.1007/s00216-011-5355-y, 2011.

734 Zhang, Q., Jimenez, J. L., Canagaratna, M. R., Allan, J. D., Coe, H., Ulbrich, I., Alfarra, M. R.,  
735 Takami, A., Middlebrook, A. M., Sun, Y. L., Dzepina, K., Dunlea, E., Docherty, K., DeCarlo, P. F.,  
736 Salcedo, D., Onasch, T., Jayne, J. T., Miyoshi, T., Shimojo, A., Hatakeyama, S., Takegawa, N., Kondo,  
737 Y., Schneider, J., Drewnick, F., Borrmann, S., Weimer, S., Demerjian, K., Williams, P., Bower, K.,  
738 Bahreini, R., Cottrell, L., Griffin, R. J., Rautiainen, J., Sun, J. Y., Zhang, Y. M. and Worsnop, D. R.:  
739 Ubiquity and dominance of oxygenated species in organic aerosols in anthropogenically-influenced  
740 Northern Hemisphere midlatitudes, *Geophys. Res. Lett.*, 34, L13801, doi:10.1029/2007GL029979, 2007.

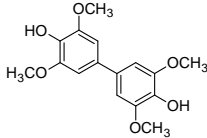
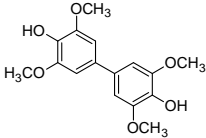
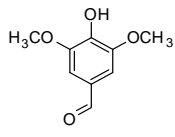
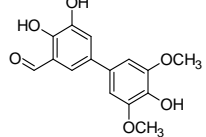
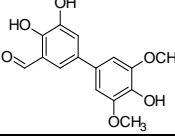
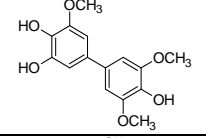
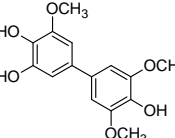
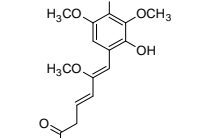
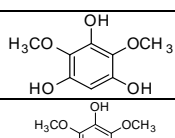
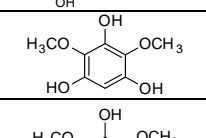
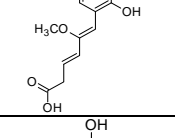
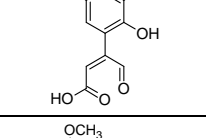
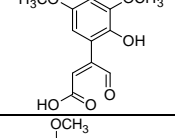
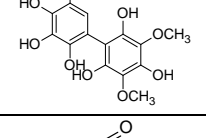
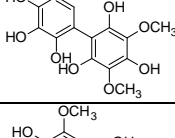
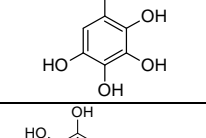
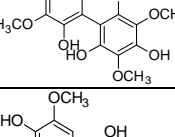
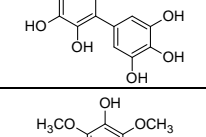
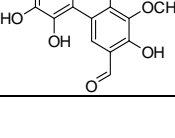
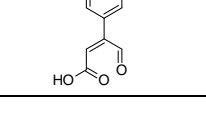
741

742 **Tables and Figures**743 **Table 1.** Summary of the chemical characteristics of phenolic aqSOA formed under different experimental conditions.  
744

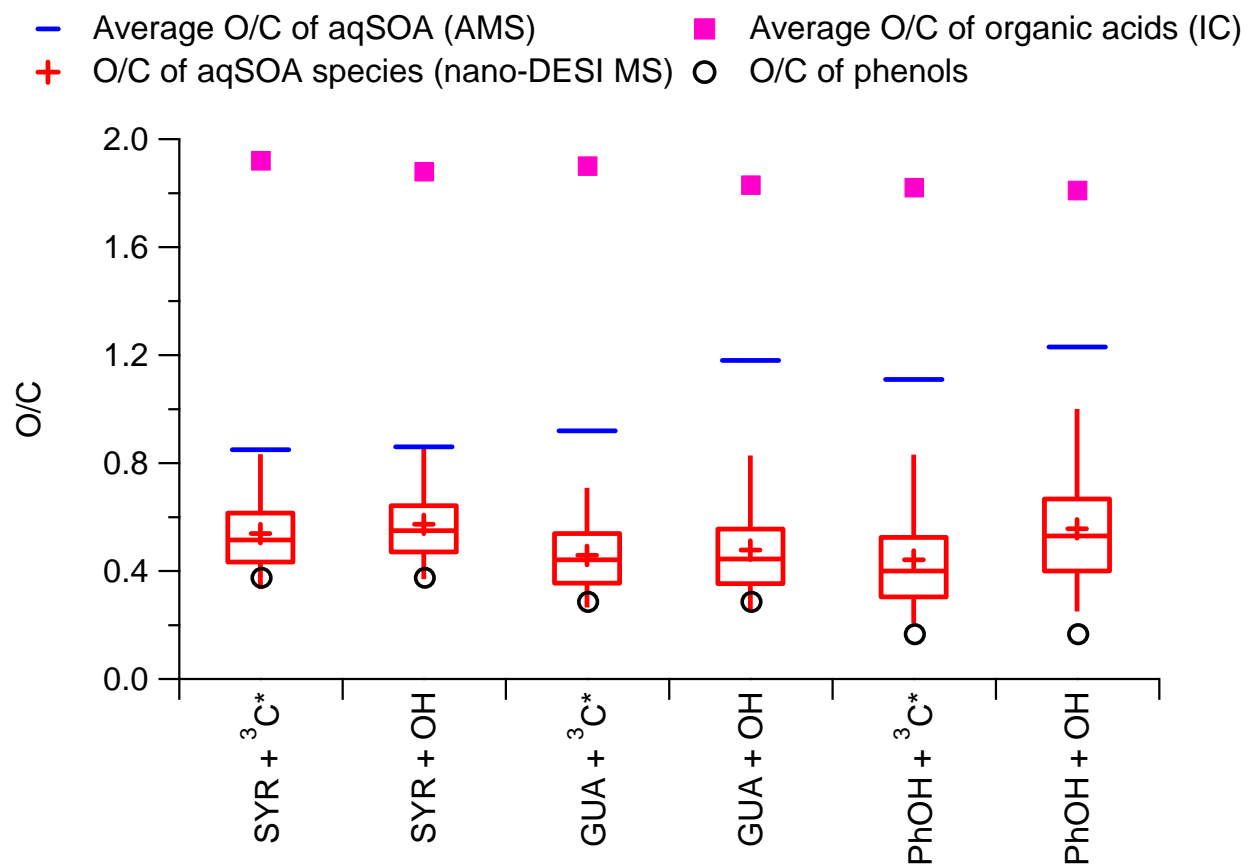
Sample information			AMS results						Nano-DESI MS results		IC results	TOC results	
Precursor	Oxidant	$t_{1/2}^a$ (min)	OM/OC	O/C	H/C	OS <sub>C</sub> <sup>b</sup>	$\Sigma m/z \geq 80^c$ (%)	Dimer <sup>d</sup> (%)	# of molecules <sup>e</sup>	# of common molecules	Organic acids (% of TOC) <sup>f</sup>	Dissolved volatile species <sup>g</sup> (%)	
Syringol (C <sub>8</sub> H <sub>10</sub> O <sub>3</sub> ) 	<sup>3</sup> C*	16	2.29	0.85	1.66	0.04	13.3	-	1156	149	0.8	6.6	
	•OH	45	2.27	0.86	1.64	0.08	12.3	-	998		0.7	5.9	
Guaiacol (C <sub>7</sub> H <sub>8</sub> O <sub>2</sub> ) 	<sup>3</sup> C*	35	2.37	0.92	1.79	0.05	14.7	0.70	827		643	0.8	4.6
	•OH	160	2.72	1.18	1.85	0.51	9.8	0.15	871		2.2	2.7	
Phenol (C <sub>6</sub> H <sub>6</sub> O) 	<sup>3</sup> C*	480	2.63	1.11	1.70	0.52	8.8	0.51	721		209	2.1	2.8
	•OH	672	2.79	1.23	1.72	0.74	6.8	0.01	445		3.8	5.7	

745  
746 <sup>a</sup>  $t_{1/2}$  is the time when approximately half of the phenolic precursor was reacted (as monitored by HPLC/UV-vis).747 <sup>b</sup> OS<sub>C</sub> indicates the oxidation state of the carbon atom ( $= 2 \times O/C - H/C$ )748 <sup>c</sup> % of total ion signal at  $m/z \geq 80$  in the AMS spectra.749 <sup>d</sup> estimated based on the signal contribution of the molecular ions of the dimers in the AMS spectra and the NIST spectra. NIST  
750 spectrum of syringol dimer is not available.751 <sup>e</sup> total number of molecules identified in the (+) ion mode and (-) ion mode nano-DESI MS spectra.752 <sup>f</sup> % of organic carbon mass in aqSOA accounted for by the sum of 8 organic acids (formate, acetate, pyruvate, malate, oxalate,  
753 malonate, fumarate, and mealete).754 <sup>g</sup> dissolved volatile species is calculated as the differences in TOC between flash-frozen and blown-down samples after correction for  
755 the mass of unreacted precursors.

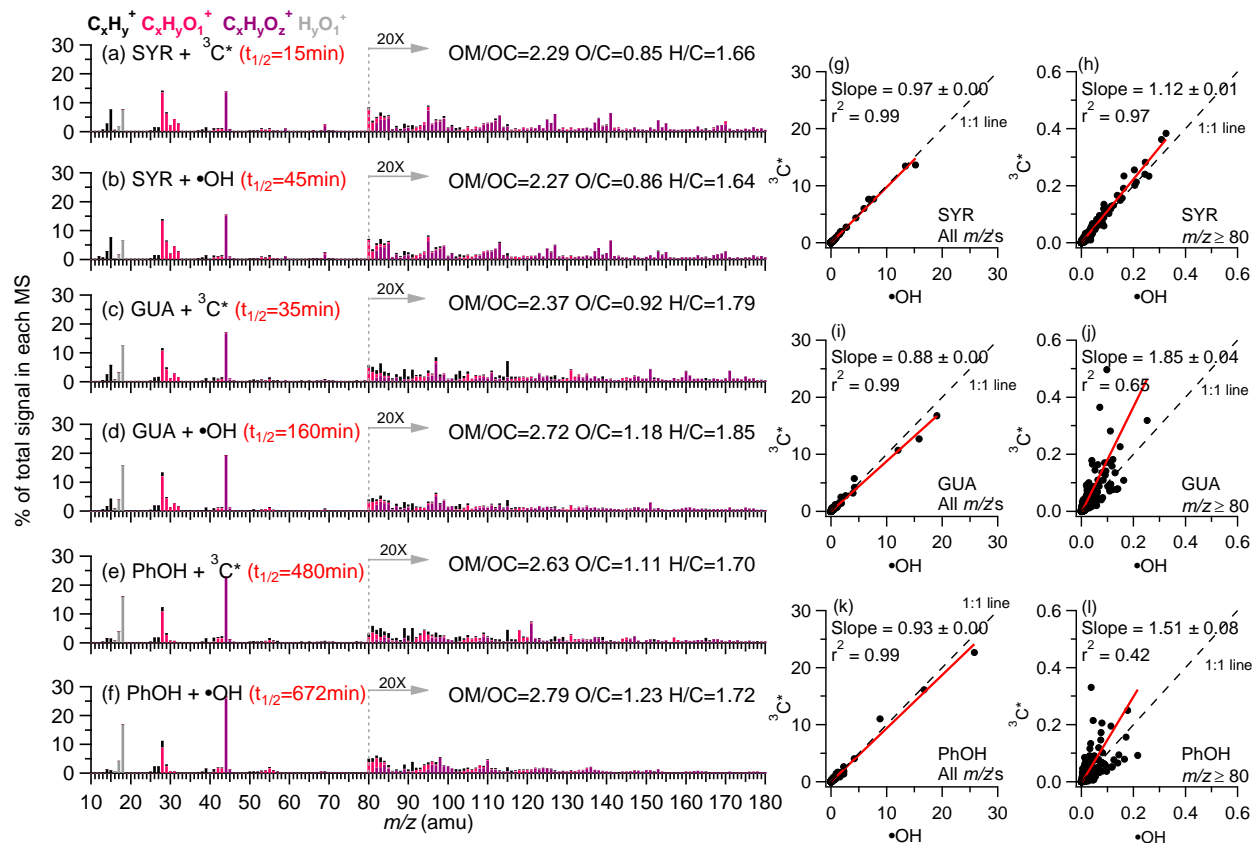
756 **Table 2.** Top 10 most abundant compounds in syringol SOA formed in  $^3\text{C}^*$ - and  $\bullet\text{OH}$ -mediated  
 757 reactions identified with (-) nano-DESI MS.

No.	$^3\text{C}^*$ reaction			$\bullet\text{OH}$ reaction		
	Molecular formula <sup>a</sup>	Proposed structure	DBE	Molecular formula <sup>a</sup>	Proposed structure	DBE
1	$\text{C}_{16}\text{H}_{18}\text{O}_6$ (306.1103)		8	$\text{C}_{16}\text{H}_{18}\text{O}_6$ (306.1103)		8
2	$\text{C}_9\text{H}_{10}\text{O}_4$ (182.0579)		5	$\text{C}_{15}\text{H}_{14}\text{O}_6$ (290.0790)		9
3	$\text{C}_{15}\text{H}_{14}\text{O}_6$ (290.0790)		9	$\text{C}_{15}\text{H}_{16}\text{O}_6$ (292.0946)		8
4	$\text{C}_{15}\text{H}_{16}\text{O}_6$ (292.0946)		8	$\text{C}_{15}\text{H}_{18}\text{O}_7$ (310.1052)		7
5	$\text{C}_8\text{H}_{10}\text{O}_5$ (186.0528)		4	$\text{C}_8\text{H}_{10}\text{O}_5$ (186.0528)		4
6	$\text{C}_{15}\text{H}_{18}\text{O}_7$ (310.1052)		7	$\text{C}_{12}\text{H}_{12}\text{O}_7$ (268.0583)		7
7	$\text{C}_{12}\text{H}_{12}\text{O}_7$ (268.0583)		7	$\text{C}_{15}\text{H}_{16}\text{O}_9$ (340.0794)		8
8	$\text{C}_{15}\text{H}_{16}\text{O}_9$ (340.0794)		8	$\text{C}_7\text{H}_6\text{O}_5$ (170.0215)		5
9	$\text{C}_{16}\text{H}_{18}\text{O}_9$ (354.0950)		8	$\text{C}_{12}\text{H}_{10}\text{O}_7$ (266.0426)		8
10	$\text{C}_{15}\text{H}_{14}\text{O}_8$ (322.0688)		9	$\text{C}_{12}\text{H}_{12}\text{O}_6$ (252.0634)		7

758  
 759 <sup>a</sup> Molecular formula of top 10 most abundant compounds with their exact mass in the  
 760 parenthesis.



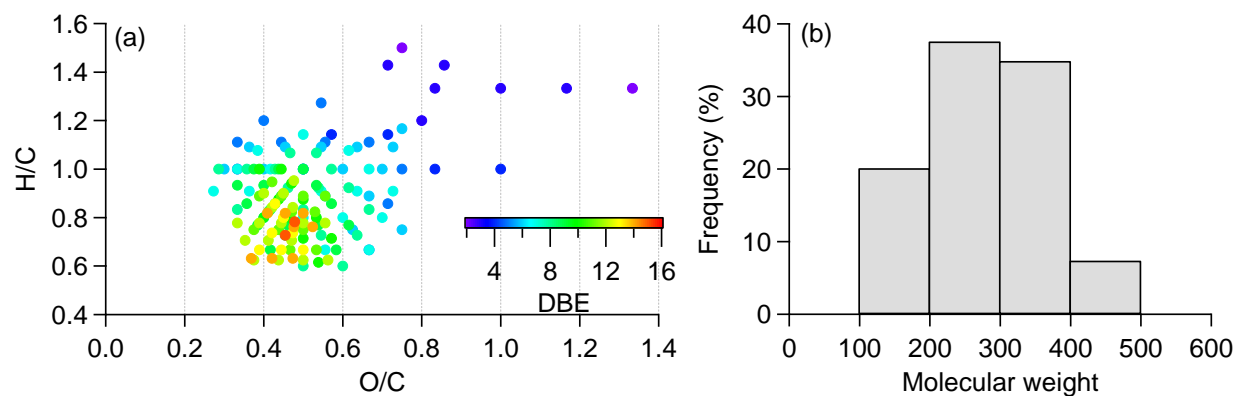
761  
 762 **Figure 1.** The average O/C ratios of aqSOA formed from the reactions of syringol  
 763 (SYR), guaiacol (GUA), and phenol (PhOH) with <sup>3</sup>C\* and •OH, respectively determined by  
 764 AMS (blue bars) and the average O/C of organic acids determined by IC (pink squares). The  
 765 distributions of the O/C of individual molecules in the aqSOA determined by nano-DESI MS are  
 766 shown in box plots, in which the whiskers above and below the boxes indicate the 95th and 5th  
 767 percentiles, the upper and lower boundaries of the boxes indicate the 75th and 25th percentiles,  
 768 and the lines in the boxes indicate the median values and the cross symbols indicate the mean  
 769 values. The O/C of the precursors are shown as black circles.



770

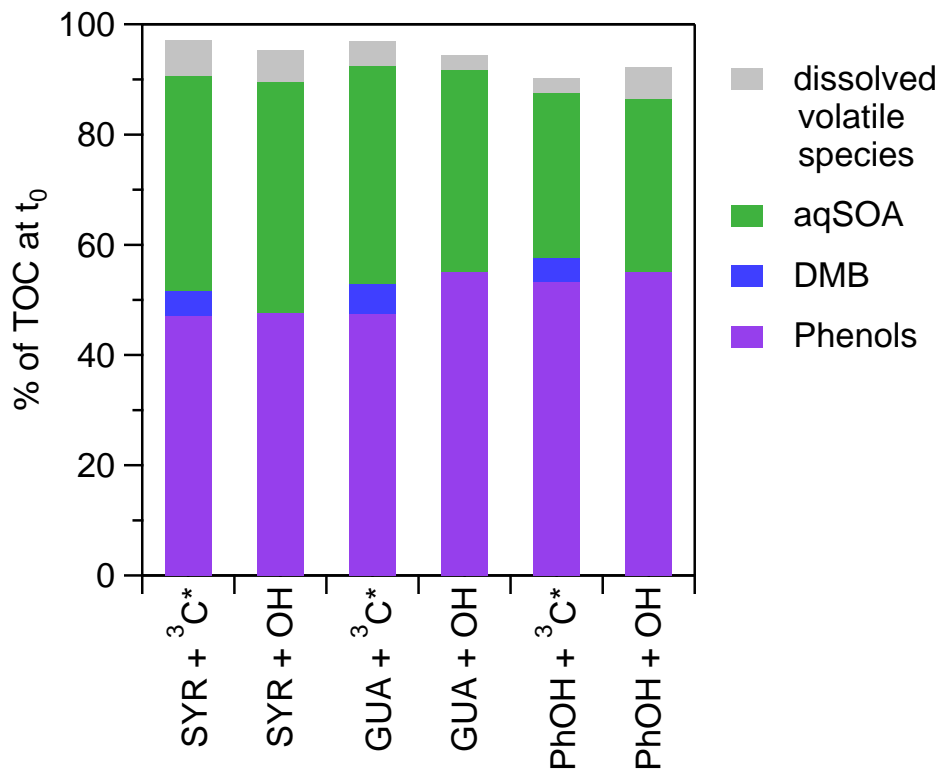
771 **Figure 2.** AMS spectra of aqSOA formed from the reactions of (a-b) syringol (SYR), (c-  
 772 d) guaiacol (GUA), and (e-f) phenol (PhOH) with  $^3C^*$  and  $\bullet OH$ , respectively. The peaks are  
 773 color-coded according to four ion categories:  $C_xH_y^+$ ,  $C_xH_yO_1^+$ ,  $C_xH_yO_z^+$ , and  $H_yO_1^+$  ( $x \geq 1$ ;  $y \geq 0$ ;  
 774  $z \geq 2$ ). The ion signals at  $m/z \geq 80$  are enhanced by a factor of 20 for clarity. The photoreaction  
 775 time and the elemental ratios of the aqSOA are shown in the legends. Scatter plots that compare  
 776 the mass spectra of aqSOA formed from two different oxidants for all  $m/z$ 's (g, i, k) and for  $m/z$   
 777  $\geq 80$  (h, j, l) were performed using the orthogonal distance regression (ODR). The linear  
 778 regression slopes and correlation coefficients are shown in the legends.





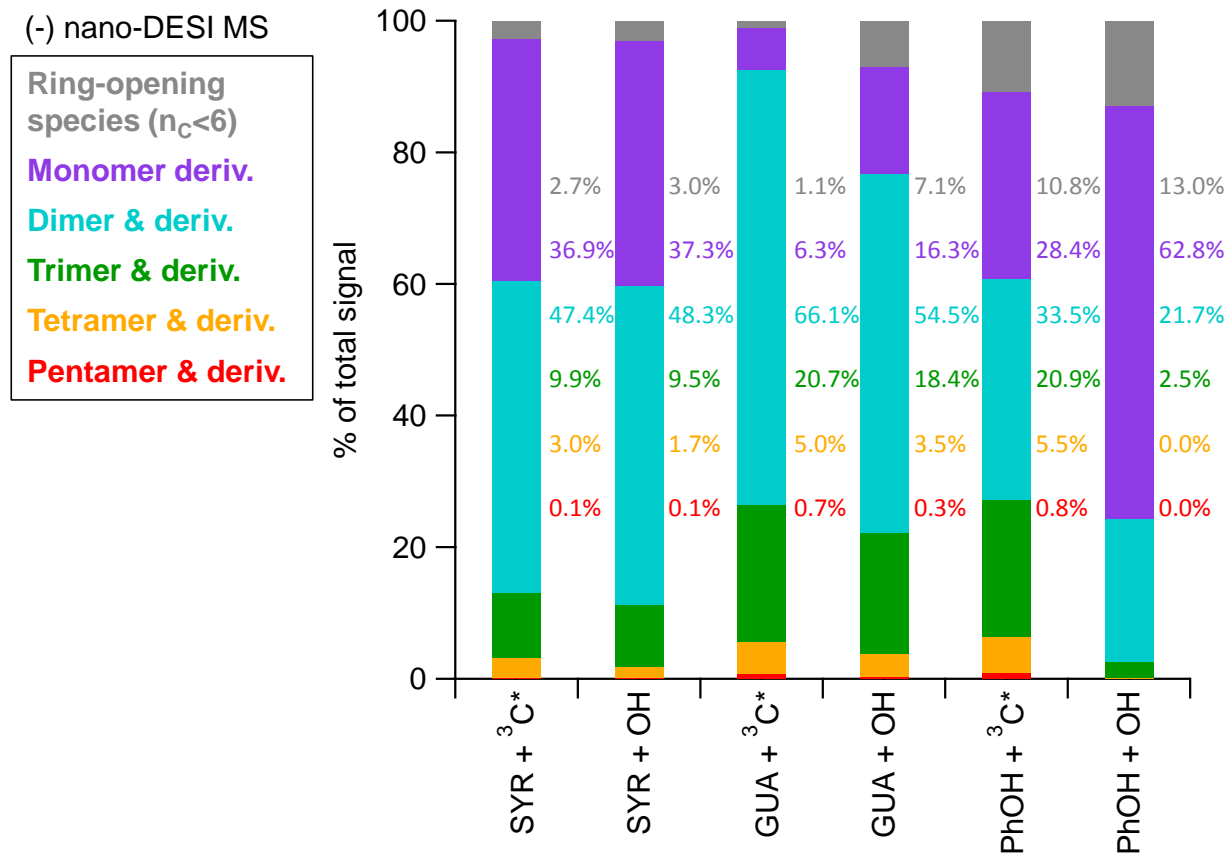
779

780 **Figure 3.** (a) Van Krevelen diagram of common molecules identified in every phenolic  
781 aqSOA via nano-DESI MS analysis. Each data point is colored by its DBE value. (b) A  
782 frequency histogram of the molecular weight of these common molecules.



783

784 **Figure 4.** Contributions of reactants (phenolic precursor and DMB) and products  
 785 (dissolved volatile species and aqSOA) to the solution TOC after illumination to  $t_{1/2}$ . TOC  
 786 amounts are expressed relative to the TOC in the initial solution prior to illumination (i.e., at  $t_0$ ).



787

788 **Figure 5.** The signal weighted distributions of syringol (SYR), guaiacol (GUA) and

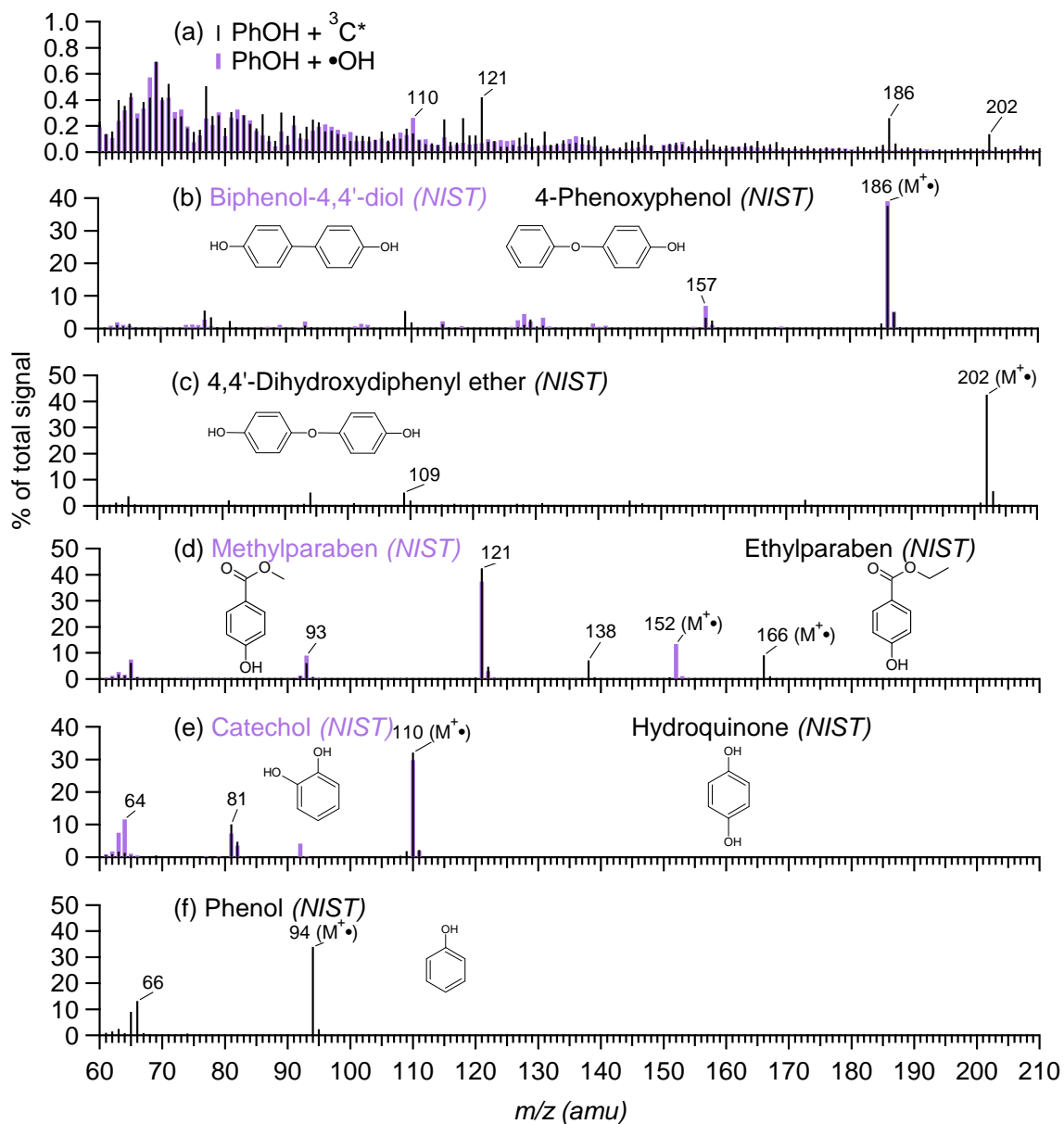
789 phenol (PhOH) aqSOA formed in  $^3C^*$ - and  $\bullet OH$ -mediated reactions, respectively, based on the

790 degree of oligomerization. The data are from the (-) nano-DESI MS spectra. Note that hexamer

791 and derivatives are only found in (+) nano-DESI MS spectrum for GUA aqSOA initiated with

792  $^3C^*$  and (-) nano-DESI MS spectrum for PhOH aqSOA initiated with  $^3C^*$ . The numbers indicate

793 the contributions of individual categories to the total signals for each sample.



794

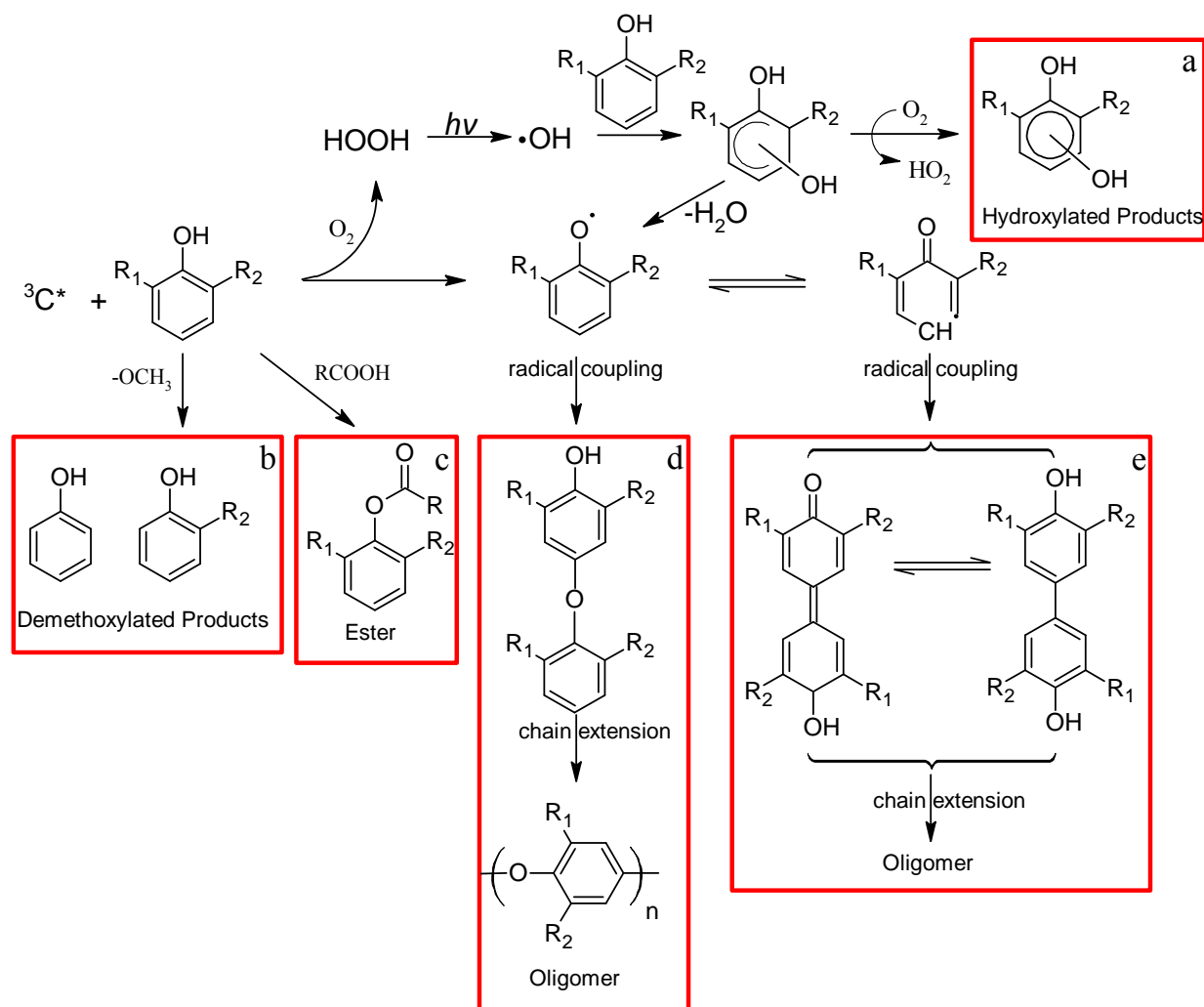
795 **Figure 6.** Comparisons between (a) the AMS mass spectra (in integer  $m/z$ ) of phenol

796 (PhOH) aqSOA formed via reactions with  $^3\text{C}^*$  and  $\bullet\text{OH}$ , respectively, and the NIST mass spectra

797 of (b) biphenol-4,4'-diol and 4-phenoxyphenol, (c) 4,4'-dihydroxydiphenyl ether, (d)

798 methylparaben and ethylparaben, (e) catechol and hydroquinone, and (f) phenol. The chemical

799 structures for each compound are shown and the molecular ions ( $\text{M}^{\bullet+}$ ) are marked.



800

801 **Figure 7.** A schematic illustrates the formation of hydroxylated species, dimers and

802 higher oligomers, esters, and demethoxylated products from aqueous photooxidation of phenolic

803 compounds. Species produced via pathways **a - e** may undergo further ring-opening processes to

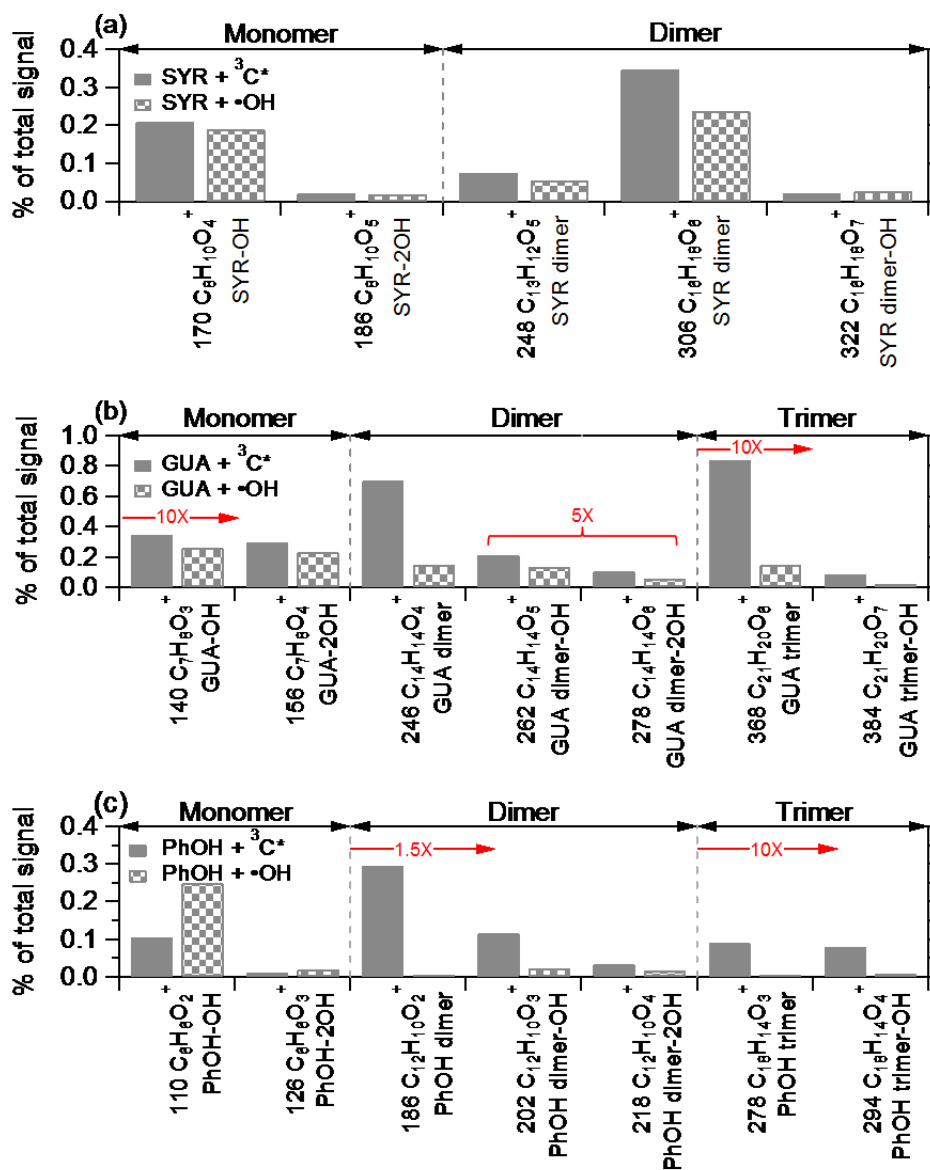
804 form ketones and carboxylic acids. Phenol:  $\text{R}_1=\text{H}$ ,  $\text{R}_2=\text{H}$ ; Guaiacol:  $\text{R}_1=\text{OCH}_3$ ,  $\text{R}_2=\text{H}$ ; Syringol:

805  $\text{R}_1=\text{OCH}_3$ ,  $\text{R}_2=\text{OCH}_3$ . Note that while radical coupling here is shown through the carbon

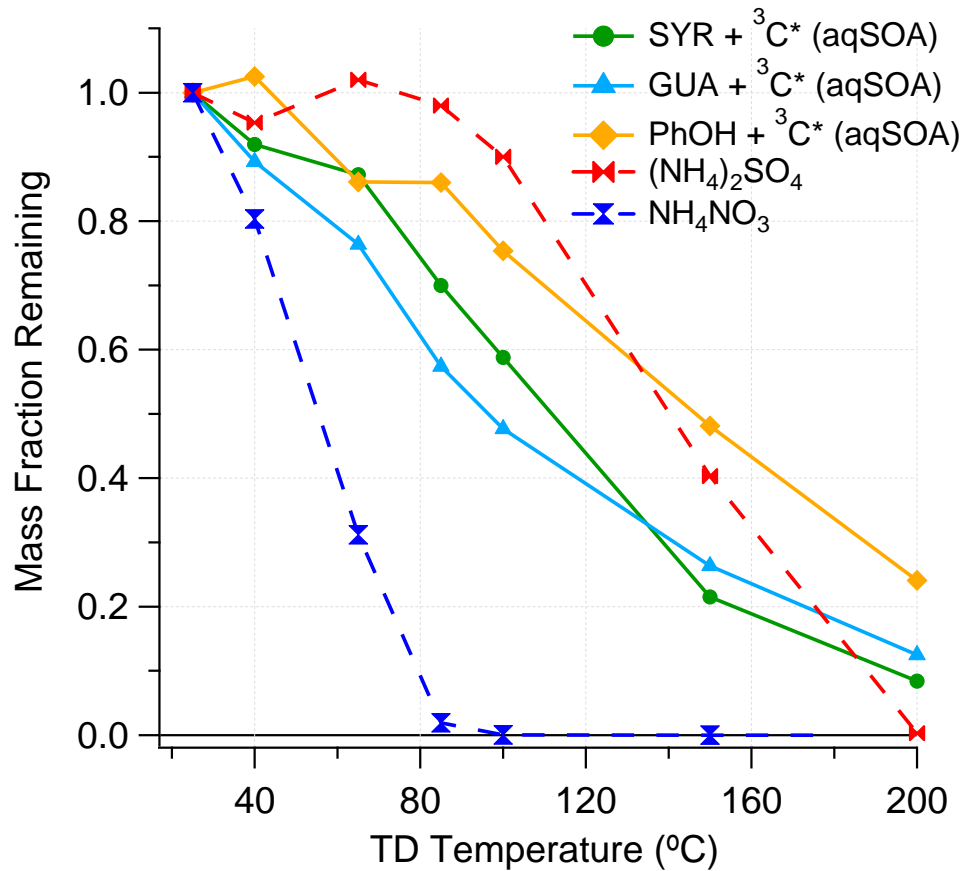
806 opposite (para) the phenoxy group, other geometric isomers will also be formed during these

807 reactions.

808



809  
 810 **Figure 8.** Comparisons of the relative abundances of signature ions in the AMS spectra  
 811 of the aqSOA of (a) syringol (SYR), (b) guaiacol (GUA), and (c) phenol (PhOH) produced from  
 812 <sup>3</sup>C\*- and •OH-mediated reactions. The signal contributions of certain signature ions are  
 813 enhanced for clarity. The *m/z* values of the signature ions are shown in front of the ion formula in  
 814 the x-axes. Identities of possible parent compounds are shown to the right. 2OH represents 2  
 815 additional hydroxyl groups attached to the aromatic ring.



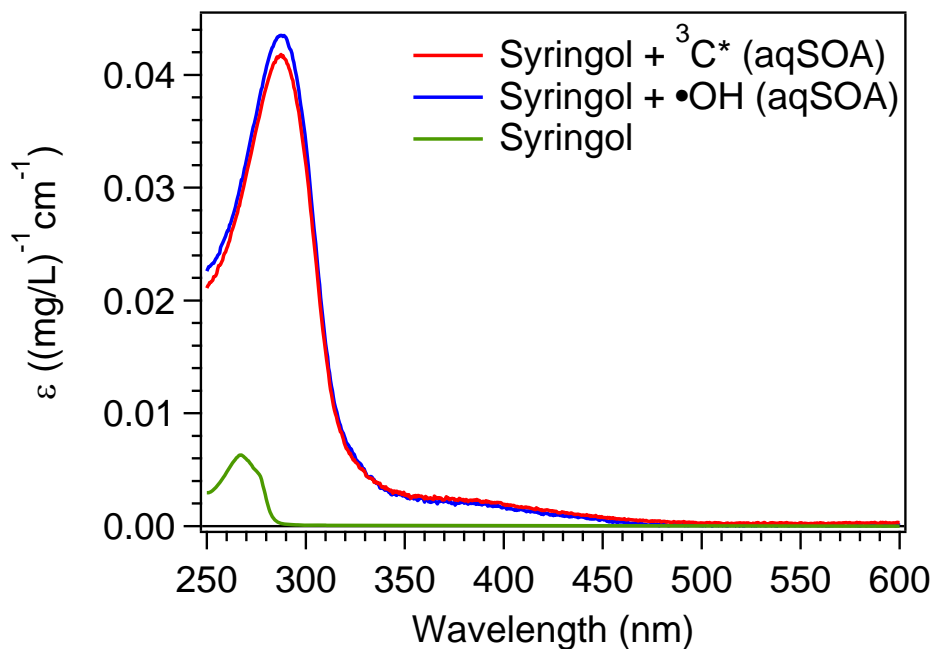
816

817

818

819

**Figure 9.** Mass thermograms of ammonium sulfate ((NH<sub>4</sub>)<sub>2</sub>SO<sub>4</sub>), ammonium nitrate (NH<sub>4</sub>NO<sub>3</sub>), syringol (SYR), guaiacol (GUA) and phenol (PhOH) aqSOA formed in <sup>3</sup>C\*-mediated aqueous-phase reactions.



820

821 **Figure 10.** UV-vis spectra of syringol and syringol aqSOA formed in  $^3\text{C}^*$ - and  $\bullet\text{OH}$ -  
 822 mediated aqueous-phase reactions. The aqSOA spectra were corrected for absorbance  
 823 contributions from unreacted reactants (syringol and DMB).